PCCP

PAPER

View Article Online
View Journal | View Issue

Cite this: *Phys. Chem. Chem. Phys.*, 2017, **19**, 31692

Shedding light on the different behavior of ionic and nonionic surfactants in emulsion polymerization: from atomistic simulations to experimental observations†

Giulia Magi Meconi,[a] Nicholas Ballard,[a] José M. Asua[a] and Ronen Zangi *[bc]

Although surfactants are known to play a vital role in polymerization reactions carried out in dispersed media, many aspects of their use are poorly understood, perhaps none more so than the vastly different action of ionic and nonionic surfactants in emulsion polymerization. In this work, we combine experimental measurements of emulsion polymerization of styrene with atomistic molecular dynamics simulations to better understand the behavior of surfactants at monomer/polymer–water interfaces. In a batch emulsion polymerization of styrene, the nonionic surfactant Disponil AFX 1080 leads to two nucleation periods, in contrast to the behavior observed for the ionic surfactant SDS. This can be explained by the absorption of the nonionic surfactant into the organic phase at the early stages of the polymerization reaction which is then released as the reaction progresses. Indeed, we find that the partition coefficient of the surfactant between the organic phase and water increases with the amount of monomer in the former, and preferential partitioning is detected to organic phases containing at least 55% styrene. Results from molecular dynamics simulations confirm that spontaneous dissolution of the non-ionic surfactant into a styrene-rich organic phase occurs above a critical concentration of the surfactant adsorbed at the interface. Above this critical concentration, a linear correlation between the amount of surfactant adsorbed at the interface and that absorbed inside the organic phase is observed. To facilitate this absorption into a completely hydrophobic medium, water molecules accompany the intruding surfactants. Similar simulations but with the ionic surfactant instead did not result in any absorption of the surfactant into a neat styrene phase, likely because of its strongly hydrophilic head group. The unusual partitioning behavior of nonionic surfactants explains a number of observable features of emulsion polymerization reactions which use nonionic surfactants and should help with future development of processes for improved control over polymerization.

Received 1st August 2017,
Accepted 5th November 2017

DOI: 10.1039/c7cp05206e

rsc.li/pccp

Introduction

Following the development of emulsion polymerization in the mid 20th century, extensive research has been conducted into the fundamental mechanistic interpretation of this complex, multiphase reaction system.[1–3] However, despite substantial effort, certain aspects of emulsion polymerization remain a 'black box', which are dealt with on a trial-and-error basis. One area in particular that remains poorly understood is the influence of surfactant structure on the emulsion polymerization process. Surfactants are a vital component of emulsion polymerization, which serve both to nucleate particles during the polymerization and also to provide a barrier to coagulation of the latex during synthesis and storage. However, in many applications the surfactant causes significant problems and its use must therefore be carefully regulated. For example, in adhesive films cast from polymer dispersions the surfactant tends to migrate towards to the polymer–air interface, resulting in increased water sensitivity and poor substrate adhesion.[4]

The most commonly used surfactants in emulsion polymerization can be classified into two groups; on the one hand ionic surfactants such as sodium dodecyl sulfate (SDS), and on the other nonionic surfactants, most of which are fatty alcohol ethoxylates. The use of ionic surfactants is usually associated with rapid nucleation of particles, which is necessary to achieve

[a] *POLYMAT & Departamento de Química Aplicada, Facultad de Ciencias Químicas, University of the Basque Country UPV/EHU, Avenida de Tolosa 72, 20018, Donostia-San Sebastián, Spain*
[b] *POLYMAT & Departamento de Química Orgánica I, University of the Basque Country UPV/EHU, Avenida de Tolosa 72, 20018, Donostia-San Sebastián, Spain*
[c] *IKERBASQUE, Basque Foundation for Science, María Díaz de Haro 3, 48013 Bilbao, Spain. E-mail: r.zangi@ikerbasque.org*

† Electronic supplementary information (ESI) available. See DOI: 10.1039/c7cp05206e

reasonable rates of polymerization, but latexes formed using these surfactants provide poor colloidal stability in high ionic strength media and poor freeze–thaw stability. Conversely, nonionic surfactants provide good colloidal stability with regards to high ionic strength media and freeze–thaw cycles, but generally result in low rates of particle nucleation and limited control of particle size. While the nucleation behavior in emulsion polymerization using ionic surfactants is generally well described by the theory of Smith and Ewart,[5] the particle nucleation behavior of nonionic surfactants shows substantial deviations from this fundamental work and the origin of these differences has been scarcely explored.

Piirma and coworkers were among the first to undertake a comprehensive study of emulsion polymerization in the presence of nonionic surfactants.[6] Using the emulsifier Emulphogene BC-840 (with a 13 carbon hydrophobic chain and 15 ethylene oxide units) in the emulsion polymerization of styrene, they observed two distinct rate regimes in the time-conversion plot as well as bimodal molecular weight distribution and bimodal particle size distribution. Later, these authors demonstrated experimental evidence to suggest that the cause of the bimodality was a change in the nature of the emulsion. They proposed that in the early stages of the reaction a water-in-oil emulsion was formed and a large fraction of the emulsifier was present in the monomer phase. As the amount on monomer decreased a phase inversion occurred and an oil in water emulsion was formed which marked the onset of the second rate regime and the generation of a crop of new particles.[7] Using Triton X-405 (with an octyl phenyl hydrophobic chain and 40 ethylene oxide units) as nonionic surfactant in the emulsion polymerization of styrene, Özdeğer *et al.* observed similar experimental results of two kinetic regimes and a bimodal particle size distribution, but offered a different explanation for the underlying cause for this phenomenon.[8] They proposed that the surfactant partitioned/absorbed into the organic phase and attributed the second nucleation period to the release of surfactant from monomer droplets as the reaction progressed. Based on results with varying concentrations of surfactant, it was suggested that the latest secondary nucleation occurred at the point at which monomer droplets disappeared ($\sim$40% conversion in the emulsion polymerization of styrene), thus assuming no absorption of the surfactant into the polymer particles. Later, Okubo and coworkers showed that absorption of the surfactant into polymer particles is often of great importance, even at high conversion,[9] and have used this advantageously in the synthesis of hollow particles, which can form as a result of surfactant induced absorption of water into polymer particles.[10,11]

In our previous work, we have demonstrated stark differences in the behavior of ionic and nonionic surfactants in emulsion polymerization, which could be attributed to the different adsorption behavior at polymer surface.[12] It was observed that the strength of adsorption of nonionic surfactants was significantly higher than ionic surfactants, and was also strongly dependent on the density of surfactant adsorbed to the surface. Using atomistic molecular dynamics (MD) simulations, these results were later explained in terms of the differences in interactions of the polar group of the surfactant (sulfate in the case of SDS and poly(ethylene glycol) in the case of the nonionic surfactant) with the aqueous phase at varying surfactant density.[13] The use of atomistic MD simulations was particularly useful in that they provided an insight into fundamental behavior at the molecular level which is not possible experimentally. Nevertheless as of yet, the vast majority of the computational studies of surfactants are limited to the behavior at interfaces[14–17] and/or inside aqueous solutions,[18–21] whereas the behavior inside an organic phase has been overlooked.

Inspired by previous experimental studies of emulsion polymerization in the presence of ionic and nonionic surfactants, in this work we investigate the different behavior of the two types of surfactant during the polymerization process as the organic phase shifts from being a monomer-rich liquid to a polymeric solid. First, an experimental study of two surfactants, SDS and Disponil AFX 1080, is performed with a focus on the differing behavior they induce with respect to particle nucleation and the effect on the polymerization process. Second, using atomistic MD simulations these results are subsequently explained and characterized by examining the differences in surfactant behavior at the interface between water and an organic phase with varying binary composition of styrene and poly(styrene).

Methods

Experimental details

Materials. Technical grade styrene (styrene, Quimidroga) was used as received. Sodium dodecyl sulfate (>99.5%, Aldrich) was recrystallized from an ethanol/water mixture, ammonium persulfate (APS, 99%, Aldrich), 2,2′-azodi(2-methylbutyronitrile) (>98%, Aldrich), dodecanethiol (>98%, Aldrich) and Disponil AFX 1080 (80% active content, BASF) were used as received. Doubly deionized water was used throughout the work. All other solvents were purchased from Scharlab and were of technical grade.

Latex characterization. *Z*-Average particle diameters were determined by dynamic light scattering performed on a Malvern Zetasizer ZS using a scattering angle of 173° at a standard temperature of 25 °C. Each measurement was conducted in triplicate and the average of the three values was taken. Drop shape analysis for surface tension measurements were conducted using a DataPhysics OCA contact angle system. The reported values are taken using an average of 5 measurements with different drops.

Scanning Electron Microscopy (SEM) images were obtained using a Quanta 250 FEG ESEM (FEI, Netherlands). An aluminium stub covered with mica was used as a substrate. To obtain monolayer coverage of polymer particles on the substrate, the latex was diluted to 0.1 wt% solids content. A drop of the diluted latex was placed onto the substrate which was dried. The images were recorded under high vacuum at an accelerating voltage of 10 kV.

Synthesis of low molecular weight poly(styrene). Low molecular weight poly(styrene) (PS), to enable the handling of

styrene/PS mixtures with high PS content, was synthesized by solution polymerization in the presence of high amount of chain transfer agent. Styrene (50 g), toluene (50 g), dodecanethiol (2.5 g) and 2,2′-azodi(2-methylbutyronitrile) (0.25 g) were added to a 250 mL round bottomed flask equipped with reflux condenser and nitrogen inlet and heated to 70 °C. The reaction was left for 24 h and after cooling the polymer was precipitated in MeOH. The solid was redissolved in chloroform, reprecipitated in MeOH, filtered and dried under vacuum.

Surfactant partitioning behavior. Styrene/polystyrene solutions ranging in composition from 0% polystyrene to 60% polystyrene by mass were formed by dissolving the low molecular weight polystyrene, synthesized as described above, over the course of 24 h. The partitioning behavior of the surfactants was analyzed by mixing 4 g of 20 mM aqueous surfactant solutions of SDS and Disponil AFX 1080 with 1 g of the styrene/polystyrene solution. The vials were placed in a water bath at 60 °C equipped with a shaking unit for 24 h to allow the surfactant to equilibrate with the two phases. After this time, the aqueous phase was removed and the solid content was analyzed gravimetrically. The residual solid from the aqueous phase was also subjected to ^{1}H NMR on a Bruker Avance DPX 400 MHz spectrometer in $(CD_3)_2CO$ at 25 °C. A relaxation time of 10 s was used in NMR measurements to ensure a quantitative measurement. In order to determine the distribution of ethylene oxide groups in the two phases, the average number of ethylene oxide groups in the surfactant partitioned in the aqueous phase, N_{EO}, was calculated by comparison of the integrals of the terminal methyl group of the polyethylene glycol chain at 0.9 ppm with the ethylene glycol groups at 3.6 ppm using the formula,

$$N_{EO} = \frac{I_{3.6}/4}{I_{0.9}/3}. \quad (1)$$

Batch emulsion polymerization. Batch emulsion polymerizations were carried out in a Mettler Toledo RC1 calorimeter equipped with an anchor type stirrer rotating at 150 rpm. Water (390 g), styrene (100 g) and surfactant were added to the reactor and degassed by nitrogen bubbling for 30 minutes, stirring constantly, and then heated to 75 °C. Once at reaction temperature, ammonium persulfate (1 g dissolved in 10 g water) was added in a single shot. The reaction was continued until the change in conversion was negligible as observed from the heat flow. Conversion of monomer as a function of time was determined from the evolution of heat flow during the reaction. At selected time intervals samples of the reaction were taken for particle size and surface tension measurements. The formulations for the batch reactions carried out are given in Table 1.

Semi-batch emulsion polymerization. Semi-batch emulsion polymerizations were carried out in a 500 mL glass reactor equipped with an anchor type stirrer rotating at 150 rpm. Water (390 g) and surfactant were added to the reactor and degassed by nitrogen bubbling for 30 minutes, stirring constantly, and then heated to 75 °C. Once at reaction temperature, ammonium persulfate (1 g dissolved in 10 g water) was added in a single shot and styrene (100 g) was fed over the course of 3 h. At the end of the feeding period the reaction was held at 75 °C for an additional 2 h in order to achieve full monomer conversion. At selected time intervals samples of the reaction were taken for conversion, particle size and surface tension measurements. Conversion of monomer as a function of time was determined gravimetrically. The formulations for the semi-batch reactions carried out are given in Table 2.

Table 1 Recipes for batch emulsion polymerization of styrene using ionic (SDS) and nonionic (Disponil AFX 1080) surfactants

	Water [g]	Styrene [g]	APS [g]	SDS [g]	Disponil AFX 1080 [g]
Run 1	400	100	1	0.58 (5 mM)	—
Run 2	400	100	1	1.15 (10 mM)	—
Run 3	400	100	1	2.30 (20 mM)	—
Run 4	400	100	1	—	3.20 (10 mM)
Run 5	400	100	1	—	6.40 (20 mM)
Run 6	400	100	1	—	12.80 (40 mM)

Table 2 Recipes for semi-batch emulsion polymerization of styrene using ionic (SDS) and nonionic (Disponil AFX 1080) surfactants

	Water [g]	Styrene [g]	APS [g]	SDS [g]	Disponil AFX 1080 [g]
Run 7	400	100	1	2.30 (20 mM)	—
Run 8	400	100	1	—	6.40 (20 mM)

Computational details

We conducted simulations of the adsorption of non-ionic surfactants at the interface between water and an organic phase. Five different organic phases with different compositions of PS and styrene (S) were considered: 100% PS, 75% PS/25% S, 50% PS/50% S, 25% PS/75% S, and 100% S. For each type of organic phase we performed several simulations corresponding to different concentrations of the surfactant. The nonionic surfactant used, 10PEO6PE, is a block copolymers of 10 units of poly(ethylene oxide) (PEO) and 6 units of poly(ethylene) (PE). In addition, to compare the behavior observed with that for ionic surfactants, simulations with SDS molecules were performed as well. In Tables S1 and S2 of the ESI† we report the details of these simulations, and in Tables S4–S7 and Fig. S1–S4 (ESI†) we provide the force-field parameters describing the (explicit-hydrogen all-atom) models for the surfactants and organic phase.

In order to prepare the starting conformations, the organic phase was pre-equilibrated as a bulk for 40 ns before the addition of surfactants and water. Then, this organic phase was placed in the middle of a rectangular box, larger along the z-axis, and surfactants (in extended conformations in which their long-axis normal and their tail point to the organic phase) were equally distributed on each side of its two interfaces. The region in the simulation box which does not include styrene or PS was then filled with water molecules described by the TIP4P-Ew model.[22] Note that certain properties deducted from simulations of charged surfactants can be sensitive to the choice of the water model. This is noticeable only at high concentrations of ionic surfactants at the interface. For example, SPC/E and TIP4P-Ew water models yield very similar adsorption affinity of SDS to a polymeric surface, however, at high concentrations

there are quantitative differences.‡ [13,23] Periodic boundary conditions in all three dimensions were employed for the simulations, nevertheless, the box lengths in the *x*- and *y*-directions were large enough to ensure absence of short-range interactions of any surfactant with its periodic image. These systems were subject to an equilibration time of 100 ns. However for the 100% S systems, this time was extended to 120 ns (for 0–20 surfactants) and 150 ns (for 30–120 surfactant) due to the miscibility of the surfactants, above a critical concentration, in the organic phase. Then, the simulations were continued for additional 20 ns for data collection. The amount of surfactants at the interface is reported by the two dimensional density, $\rho_{2D} = m/2A$, where m is the mass of the surfactants and A is the area of the simulation box in the *xy*-plane. The location of the interface was determined by a drop of the water density to half of its value in the bulk, *i.e.*, to $\sim$500 kg m^{-3}.

The calculations and the preparations of the systems for the Potential of Mean Force (PMF) of pulling one adsorbed surfactant from the interface to the water phase were done according to the protocol described in our previous study.[13] In brief, the reaction coordinate was described by the (shortest) distance, d_c, between the interface and a carbon atom of the hydrophobic tail of the surfactant covalently bonded to the oxygen atom of the hydrophilic head (see Fig. S3 and S4, ESI†). In practice, the distance involving this carbon atom of the surfactant was constrained relative to the center of mass of a cylindrical cut of the organic phase, and only during analysis a shift to represent the distance relative to the interface was applied. For several distances along the reaction coordinate, the system was equilibrated for a time period in the range of 14 ns to 50 ns (depending on the time the system displayed convergence of the constrained force). The average force that was required to constrain the distance between the reference and the pull group was calculated in a data collection step of additional 36 ns. To obtain the PMF (or free/Gibbs energy profile), this average force was integrated as a function of the constrained distance, d_c. Because the PMF represents only relative values, it was shifted such that the Gibbs energy of the state at the largest separation corresponds to zero. Note that in these series of simulations, only one interface between the organic phase and water was initially adsorbed with surfactants. Further details on this series of simulations are given in Table S3 (ESI†).

All computer simulations were performed using the molecular dynamics package GROMACS version 4.6.5.[24] A constant temperature of 300 K was maintained by the velocity rescaling thermostat[25] with a coupling time of 0.1 ps. The box length along the *z*-axis was fixed during the simulation, however, in the *xy*-plane the pressure was maintained at 1.0 bar utilizing the Berendsen barostat[26] with a compressibility of 1×10^{-6} bar^{-1} and a coupling time of 1.0 ps. Electrostatic interactions were calculated using the Particle-Mesh-Ewald method.[27,28] Quadratic interpolation was used with a real space cutoff of 0.9 nm and a grid spacing for the reciprocal-space of 0.12 nm. A 0.9 nm cutoff was also used to calculate the Lennard-Jones potential applying long range dispersion corrections for the energy and pressure. Water bond distances and angles were constrained using the SETTLE algorithm,[29] whereas all-other bond distances were constrained using the LINCS algorithm.[30] A time step of 2 fs was used to integrate the equation of motion, except for simulations utilizing the pull-code (for calculating the PMFs). Constraining the distance within the pull-code resulted in occasional instabilities, which disappeared upon reduction of the time step to 1 fs. Therefore, in these simulations a 1 fs time step was used. Two molecules were considered to be hydrogen bonded if the distance between the donor (oxygen) and acceptor (oxygen) is smaller than 0.35 nm and the hydrogen–oxygen (donor)–oxygen (acceptor) interaction angle is smaller than 30°.[31] Fig. S6a and b (ESI†) indicate these values to be appropriate for our systems as well.

‡ We conjecture that different water models affect differently the extent of counterion condensation onto the assembled structure of the surfactants leading to different magnitudes of repulsive energy between the ionic head groups.

Results and discussion

In order to gain an insight into the different behavior ionic and nonionic surfactants have during emulsion polymerization, we performed emulsion polymerization of styrene using varying quantities of an ionic surfactant, SDS (5–20 mM), and a nonionic surfactant, Disponil AFX 1080 (10–40 mM), at a solids content of 20%. The reactions were carried out in a calorimeter reactor to allow for continuous monitoring of the rate of polymerization and samples were taken periodically for measurements of the particle size and surface tension of the aqueous phase. The evolution of the heat of reaction, particle size, and surface tension as a function of conversion, for various concentrations of SDS, are shown in Fig. 1.

Fig. 1 indicates that SDS behaves as a 'classical' surfactant in the emulsion polymerization of styrene. Based on the surface tension measurements, it is evident that initially the surfactant concentration in the aqueous phase is slightly below the CMC for Run 1 and above the CMC for Runs 2 and 3, as expected based on the known CMC of SDS (8.2 mM)[32] and the concentrations of SDS used. In the early stages of the reaction, the surface tension rapidly increases in all cases as a result of micellar particle nucleation and adsorption of the surfactant to the newly formed interfaces. The surface tension reaches a steady value close to that of pure water indicating a low concentration of free surfactant in the aqueous phase. It can be observed that the particle size increases with decreasing surfactant concentration. At higher surfactant concentration the initial number of micelles in the system is higher and thus a higher number of particles are generated in the early stages of the reaction, which are consequently of lower size. The evolution of the rate of polymerization, as reflected by the heat of reaction, shows an initial rapid rate which slows to a constant value, perhaps as a result of some coalescence of particles which reduces the overall number of particles and thus the polymerization rate. As may be expected due to effects of radical compartmentalization, which results in a reduced termination

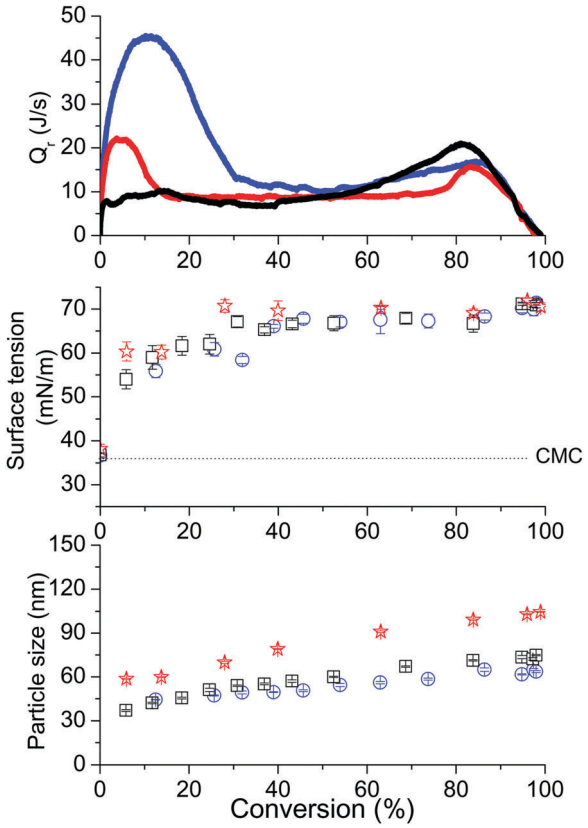

Fig. 1 Evolution of heat of reaction, surface tension and particle size as a function of conversion for emulsion polymerization of styrene with 5 mM (Run 1, red line and stars), 10 mM (Run 2, black line and squares), and 20 mM (Run 3, blue line and circles) SDS.

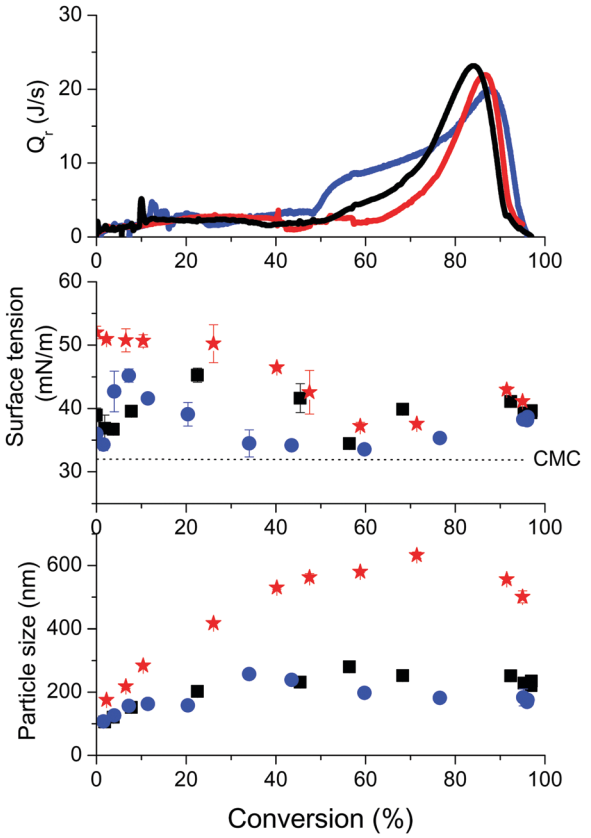

Fig. 2 Evolution of heat of reaction, surface tension and particle size as a function of conversion for emulsion polymerization of styrene with 10 mM (Run 4, red line and stars), 20 mM (Run 5, black line and squares), and 40 mM (Run 6, blue line and circles) Disponil AFX 1080.

rate for smaller particle sizes, this initial rise in the heat of polymerization is largest for the reaction containing most surfactant, where particle size is smallest. At around 80% conversion, there is a rapid increase heat of reaction which corresponds to the time at which the gel effect becomes visible.[33] In this region the rate of termination is lowered due to restricted diffusion of the propagating chains which results in an increase in the rate of polymerization.

The behavior of the nonionic surfactant Disponil AFX 1080 in the emulsion polymerization strongly differs from that of SDS Fig. 2. Despite using a concentration of Disponil AFX 1080 which is at least an order of magnitude higher than the CMC,[34] the surface tension measurements reveal that from the first moment the concentration of surfactant in the aqueous phase is below the CMC. The low concentration of surfactant in the aqueous phase leads to nucleation of fewer particles, primarily by homogeneous nucleation, which are consequently of a larger size. The nucleation period is accompanied by a decrease in the surfactant concentration in the aqueous phase for reactions with 10 and 20 mM Disponil AFX1080, because the limited amount of surfactant in the aqueous phase adsorbs to the newly formed interfaces. The relatively large size of the particles also means that in the early stages of the reaction the rate of polymerization is low as reflected by initial values for the heat of polymerization which are an order of magnitude below that of the reactions conducted using SDS as surfactant. As the reaction progresses, the concentration of surfactant in the aqueous phase increases and eventually reaches the CMC. At this point, the onset of nucleation of a second crop of much smaller particles by heterogeneous (micellar) nucleation leads to a decrease in the average particle size. Due to the increased number of particles in the system and the well known effects of radical compartmentalization in emulsion polymerization, the nucleation of new particles also results in a concomitant increase in the rate of polymerization, as is observed in the rapid increase in the heat of polymerization. With lowering the amount of surfactant in the formulation, this effect was observed at a later stage in the polymerization process. It should also be noted that contrary to the work of Özdeğer *et al.*[8] this effect could be seen to occur after the disappearance of monomer droplets (~40% for styrene) in some reactions. At high conversion, as for SDS, the gel effect is observed which is visible in the onset of a high rate of polymerization at around 80% conversion.

The appearance of a new crop of particles, arising from secondary nucleation in the emulsion polymerization of styrene, when using a nonionic surfactant is confirmed visually by scanning electron microscopy images of the final latex displayed in Fig. 3. It can be seen that latexes synthesized with SDS

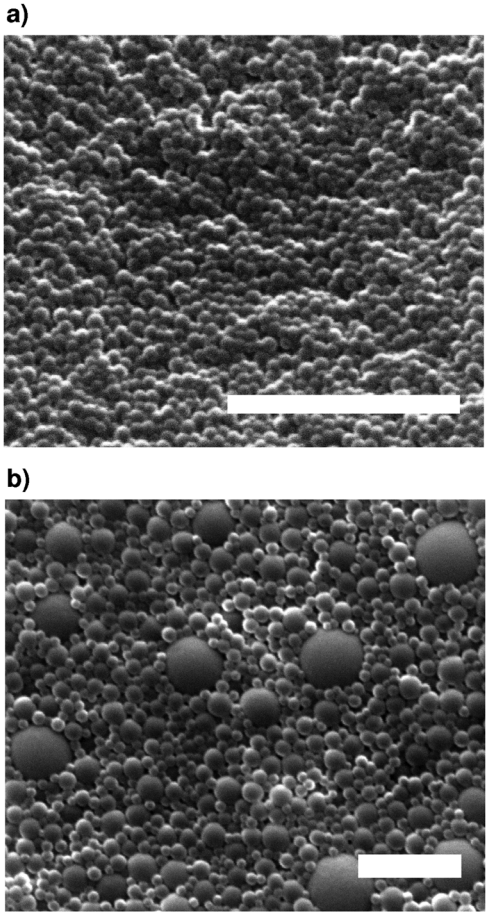

Fig. 3 SEM images of latexes synthesis using either (a) SDS (Run 3) or (b) Disponil AFX 1080 (Run 5). In both cases the white scale bar represents 1 micron.

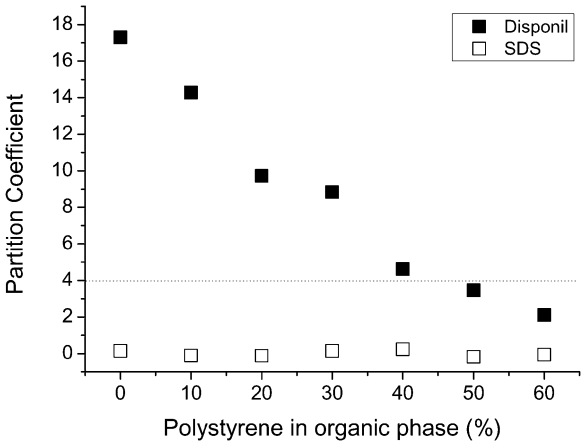

Fig. 4 Partition coefficient, as defined in eqn (2), of SDS (open symbols) and Disponil AFX 1080 (closed symbols) as a function of increasing fraction of PS in organic phase. The dotted horizontal line denotes the value of the partition coefficient at which the surfactant is partitioned equally between the water and the organic (for emulsion composition of 20% organic phase).

contain a unimodal distribution of small particles, whereas those synthesized with Disponil AFX 1080 contain one crop of large particles and a second crop of much smaller particles. The larger particles are formed at the beginning of the reaction where the aqueous phase surfactant concentration is low. The large size of these particles is in agreement with the initial low rate of polymerization as discussed above. The smaller particles are formed at the point at which the CMC is reached in the aqueous phase, which leads micellar nucleation and results in a new crop of small particles as well as the reduction in the average particle size as shown by DLS measurements (see Fig. 2).

How is it possible that the amount of (nonionic) surfactant in the aqueous phase increases during the polymerization reaction? Note that the area of the interface at which the surfactant adsorb only increases during the reaction. Similar to the conclusions reported by Özdeğer *et al.*,[8] we hypothesize that initially the surfactant is somehow partitioned into the organic phase and later, as the reaction proceeds, is released into the aqueous phase. It is therefore the purpose of this paper to confirm this hypothesis, to investigate how a surfactant with a hydrophilic head can partition into a completely hydrophobic medium, and why it is then released at later stages of the polymerization process.

We start by designing a simple direct experiment in which we measure the partition coefficient of both SDS and Disponil AFX 1080 between water and an organic phase containing various compositions of styrene and PS. The partition coefficient, P_s, was calculated by,

$$P_s = \frac{m_{s,op}/m_{op}}{m_{s,aq}/m_{aq}}, \quad (2)$$

where $m_{s,op}$ is the mass of surfactant in the organic phase and m_{op} is the mass of the organic phase. The corresponding terms for the aqueous phase are $m_{s,aq}$ and m_{aq}. Note that in this experiment it is not possible to distinguish between surfactants adsorbed at the interface to those absorbed inside the organic phase. Nevertheless, the area of the interface relative to the volume of the organic phase is very small so the amount of surfactant at the interface can be ignored. The results shown in Fig. 4 indicate that SDS resides entirely (within experimental error) in the aqueous phase. In this case, the surfactant may be expected to behave as a classical surfactant in emulsion polymerization as initially postulated by Smith and Ewart.[5] In contrast, for Disponil AFX 1080 the surfactant is present substantially in the organic phase. As the quantity of monomeric styrene in the organic phase increases the surfactant has an increasing affinity for the organic phase. Furthermore for organic phases containing less than 45% PS, the concentration of surfactant in the organic phase is larger than in water. This means that in emulsion polymerization the surfactant is partitioned not just between the aqueous phase and the polymer–water interface, but also partitions into the monomer droplets and/or the polymer particles themselves.

Note that commercially available Disponil AFX 1080 contains a distribution of surfactants characterized by different

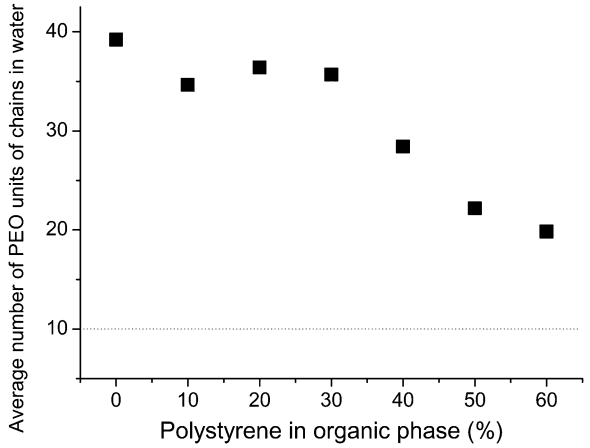

Fig. 5 Average number of ethylene oxide units of the surfactant molecules residing in the aqueous phase with increasing fraction of PS in organic phase.

lengths of the ethylene-oxide chain, albeit peaked at 10 units. These different surfactants are likely to partition differently between the two phases. By ^{1}H NMR analysis, it was possible to measure the average number of ethylene oxide groups of the surfactants in the aqueous phase (see Fig. 5). As expected, surfactants with a larger number of ethylene-oxide groups displayed a higher propensity to reside in the aqueous phase. As the amount of PS in the organic phase increases the average number of ethylene oxide units decreases approaching the value of 10.

To further examine our hypothesis that secondary nucleation is triggered by a late release of surfactants from the organic phase, we conducted an additional set of experiments under semi-batch conditions with slow addition of the monomer. Under these conditions the monomer concentration remains low throughout the experiment and the effect of surfactant partitioning should therefore be avoided. In the case of SDS the evolution of particle size and surface tension follow a similar trend to the reaction in batch, although with a much smaller particle size as a result of the low rate of particle growth (see Fig. 6).[35,36] As particles are nucleated, the concentration of surfactant in the aqueous phase is decreased due to adsorption to the newly formed water–polymer interface. The particle size is small and thus rate of polymerization is high, resulting in a high instantaneous conversion for the duration of the reaction.

In contrast, the reactions conducted using the nonionic surfactant showed very different behavior in semibatch compared to batch emulsion polymerization. In the early stage of the reaction, the concentration of surfactant is above the CMC and thus nucleation of particles decreases the amount (and thereby, the concentration) of surfactant in the aqueous phase because it adsorbs to the newly formed particles (see Fig. 7). Compared to the reaction with SDS, the particle size was larger which results in a lower rate of polymerization and as a consequence the reaction did not proceed under starved conditions, namely the concentration of monomers inside the particles was higher than for a typical semi-batch reaction.

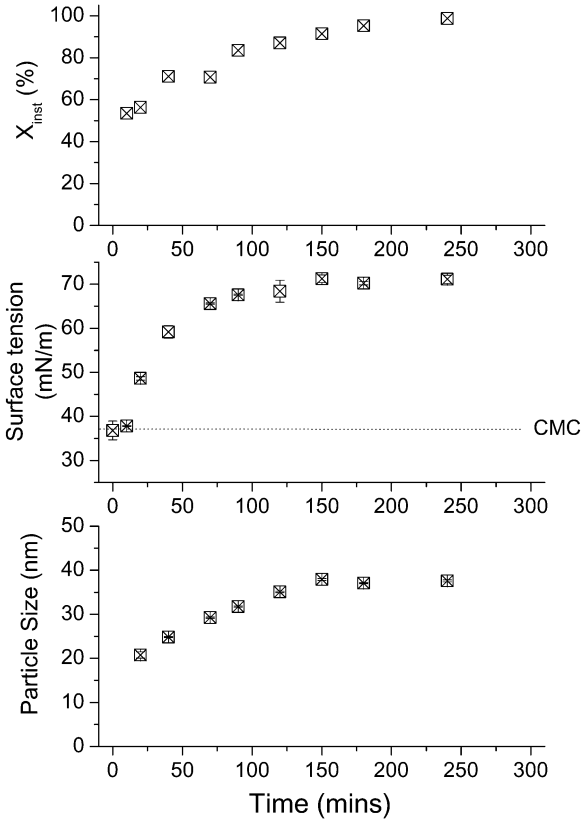

Fig. 6 Evolution of instantaneous conversion, X_{inst}, surface tension and particle size during the semi-batch emulsion polymerization of styrene using SDS as surfactant (Run 7).

For this reason, we suspect that some surfactants were able to partition to the organic phase and at later stages of the reaction were released to the aqueous phase. This explains the small reduction in surface tension at around 130 minutes in Fig. 7. Crucially however, the amount of surfactant in the aqueous phase does not reach the CMC and thus secondary nucleation does not occur. The result is a monodisperse particle size distribution standing in stark contrast to the results from batch polymerizations. The absence of any secondary nucleation in the semi-batch polymerization using Disponil AFX 1080 was further evidenced by the highly monodisperse nature of the latex as revealed by SEM (see Fig. 8).

To understand at the molecular level the absorption of a nonionic surfactant (10PEO6PE) into a styrene-rich organic phase we performed molecular dynamics (MD) simulations. First, the adsorption character of the surfactant at the organic-phase–water interface was investigated, and second, potential spontaneous absorption into the organic phase was examined. The results obtained with the nonionic surfactant were then compared to those with an ionic surfactant (SDS).

It is reasonable to assume that the absorption into a styrene-rich organic phase, and later, the release from a PS-rich phase arise because the strength of binding of the surfactant to styrene is stronger than that to PS. Therefore, in the first series of simulations we calculated the potential of mean force (PMF)

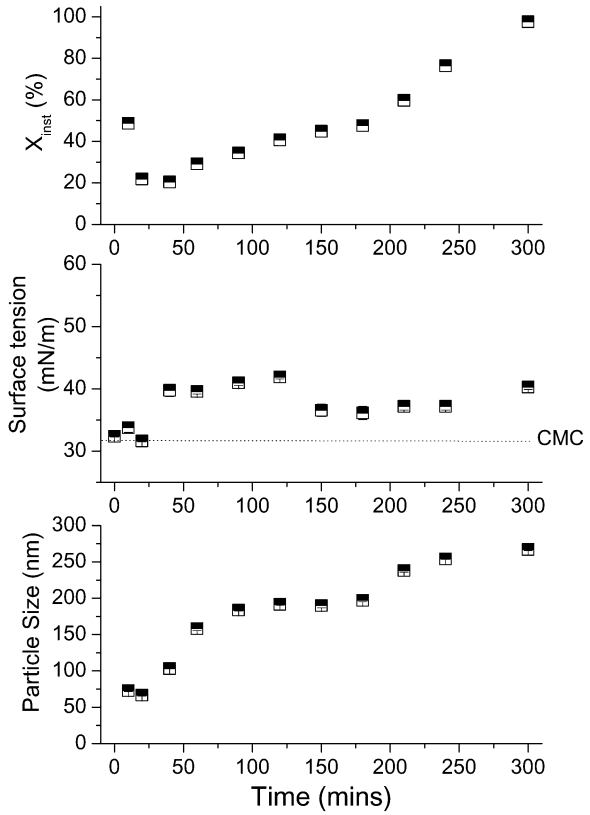

Fig. 7 Evolution of instantaneous conversion, X_{inst}, surface tension and particle size during the semi-batch emulsion polymerization of styrene using Disponil AFX 1080 as surfactant (Run 8).

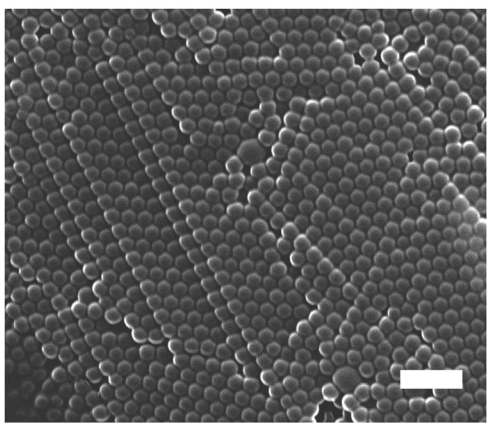

Fig. 8 SEM image of latex produced by semi-batch emulsion polymerization of styrene using Disponil AFX 1080 (Run 8). The white scale bar represents 1 micron.

of pulling an adsorbed 10PEO6PE surfactant away from the interface, towards the water phase, for three different surfactant concentrations. In this case the organic phase was either neat PS (results taken from our previous work[13]) or neat styrene. The results are shown in Fig. 9 which suggests it is not possible to attribute this peculiar behavior of the nonionic surfactant to different binding strengths. The depths of the minima of the PMFs (which occur around the same location

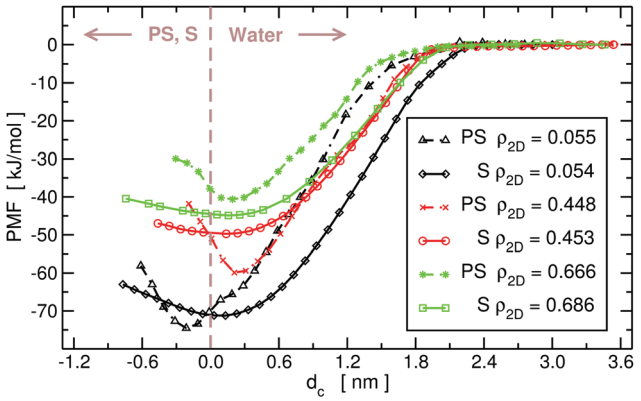

Fig. 9 The (Gibbs) free energy profile of pulling away one 10PEO6PE surfactant from the organic-phase/water interface into the water phase as a function of the constrained distance, d_c. Different curves correspond to different 2D-densities (in mg m^{-2}) of the surfactant. Dashed lines are for PS and solid lines are for styrene. The brown vertical dashed line marks the interface.

with respect to the interface) display similar values for the two organic phases, except for $\rho_{2D} \simeq 0.4$ where binding to PS is found to be stronger. Nevertheless, the shape of minima is different. Whereas for PS the minima are well defined, indicating the surfactant experience substantial penalty when pushed farther into the organic phase, for styrene the minima are very shallow and at higher concentrations are almost completely flattened. This means that at high concentrations, there is hardly any penalty for the surfactant to penetrate and adsorb at, the styrene phase. In Fig. 10 we display the last configuration at each surfactant concentration for the simulations with PS and styrene. For PS, the head groups of the surfactants are always at the PS–water interface whereas the hydrophobic tails can sometimes enter the organic phase. In contrast, for styrene at the two highest concentrations the entire 10PEO6PE surfactant penetrates the organic phase, and in fact, at the highest concentration one surfactant even passed through the whole styrene phase and adsorbed at the opposite interface that was initially devoid of surfactants. Obviously once the devoid interface becomes accessible, the concentration of the surfactant at equilibrium at both interfaces should be equal because of the 2-fold symmetry of the system. Therefore, if the starting conformation includes surfactants only at one interface the simulation time to reach equilibrium will be, unnecessarily, very long.

As a consequence, we constructed another series of simulations in which the starting configurations include the same concentration of surfactant at both interfaces. In this case, we also considered different chemical compositions of the binary organic phase, in particular, we successively increased the percentage of monomeric styrene, inside PS, in steps of 25%. These different compositions of S/PS in the organic phase correspond to different stages of the polymerization process. In Fig. 11 we display the density profiles along the z-axis for all different organic phases at surfactant density (*i.e.*, the density initially put at the interface) of $\rho_{2D} = 1.61 \pm 0.09$ mg m^{-2},

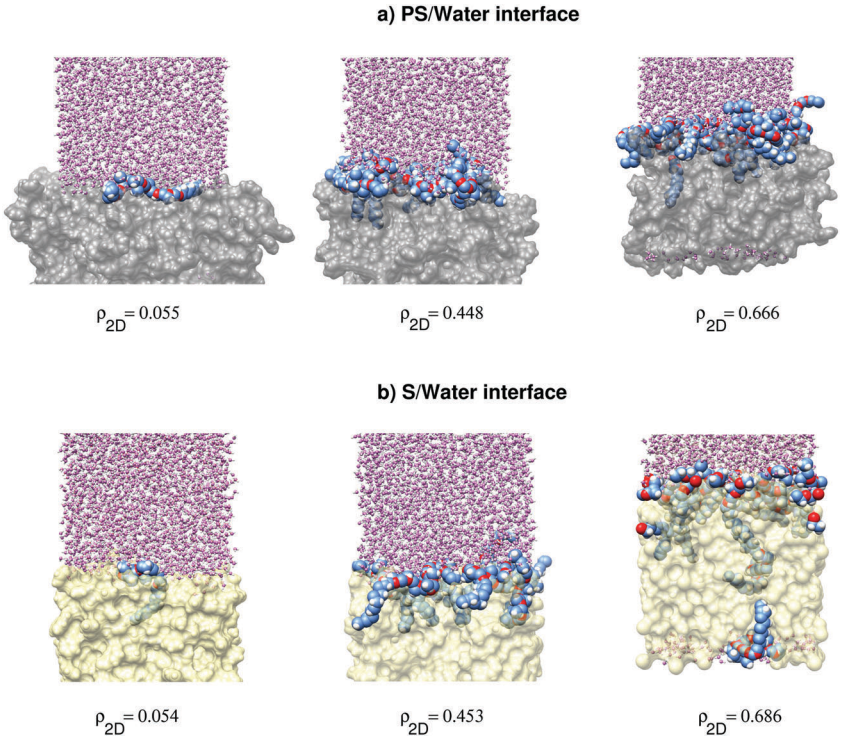

Fig. 10 Side view of instantaneous configurations of the simulation box of the 10PEO6PE surfactants adsorbed at equilibrium (*i.e.* at zero pull-force) at (a) PS/water interface and (b) styrene/water interface for the three 2D-densities (in mg m^{-2}) studied. The poly(styrene) and styrene are shown in a surface representation colored gray and beige, respectively. Water molecules are colored in pink with a ball-and-stick representation. The carbon, oxygen, and hydrogen atoms of the surfactant are shown as space filling spheres colored in blue, red, and white, respectively. For clarity, the snapshots do not capture the entire length of the simulation box along the z-axis (normal to the interface), nevertheless, the same figure displaying the entire simulation boxes is given in Fig. S7 (ESI†).

alongside snapshots of the last configuration of the corresponding simulations. For the systems with 100% PS, 75% PS, and 50% PS, the hydrophilic head and hydrophobic tail of the surfactants are at the interface where the former is positioned more towards the water phase and the latter towards the organic phase. However, a closer inspection of the density profiles of these systems reveals that the surfactants shift into the organic phase with the increase of the content of styrene. Notably, at 50% content of PS there is an onset of a second peak in the distribution of the surfactants heads that is closer to the organic phase, and a concomitant extension of the tail of the water distribution around this second peak position. These trends are augmented in 25% PS and 0% PS (*i.e.*, 100% S), however, in these two systems some of the surfactants can be clearly classified by visual inspection as being completely dissolved (or absorbed) in the organic phase. For 100% S, the density distribution of the surfactants is non-zero throughout the entire styrene phase. These are unexpected results given the common working assumption that below the CMC surfactants adsorb at the interface, and above the CMC they form micelles in the aqueous phase.

We now examine the extent of the absorption of the surfactant into the organic phase for different concentrations of surfactants initially placed at the interface. A surfactant is considered to be inside the organic phase if the z-coordinate of its first tail carbon atom (the atom covalently bonded to the oxygen atom of the head), z_s, satisfies the condition $(-z_i + 2.5\ \text{nm}) < z_s < (+z_i - 2.5\ \text{nm})$, where $+z_i$ and $-z_i$ are the intersection points the two interfaces' lines make with the z-axis. The distance of 2.5 nm away from the interfaces lines represents the region towards the organic phase that is still considered to be the interface.§ At equilibrium, the chemical potential of the surfactant at the interface equals its chemical potential inside the organic phase. This equality determines the partitioning of the surfactant into these two phases (see eqn (S3) in the ESI†), and therefore, in Fig. 12a we plot its 3D-density in the organic phase as a function of its 2D-density at the interface. For the systems of 100% PS and 75% PS, the organic phase entirely lacks any surfactant. The 50% PS (50% S) phase supports very small density of surfactant starting at $\rho_{2D} \sim 0.7$ mg m^{-2}. However as the percentage of styrene increases, *i.e.* the systems of 75% S and 100% S, there is a substantial increase in the concentration of the surfactant absorbed inside the organic phase. Nevertheless even at 100% S, there is still a critical density at the interface below which the surfactant does not absorb into the organic phase. The values of this critical density are $\rho_{2D} \sim 0.7$ and 0.3 mg m^{-2} for 75% S

§ Its value was determined from the distance in the density profile between the point the distribution of the head atoms vanishes and the interface line, for a case when no surfactant absorption was detected, *i.e.*, for the system with 100% PS as shown in Fig. 11.

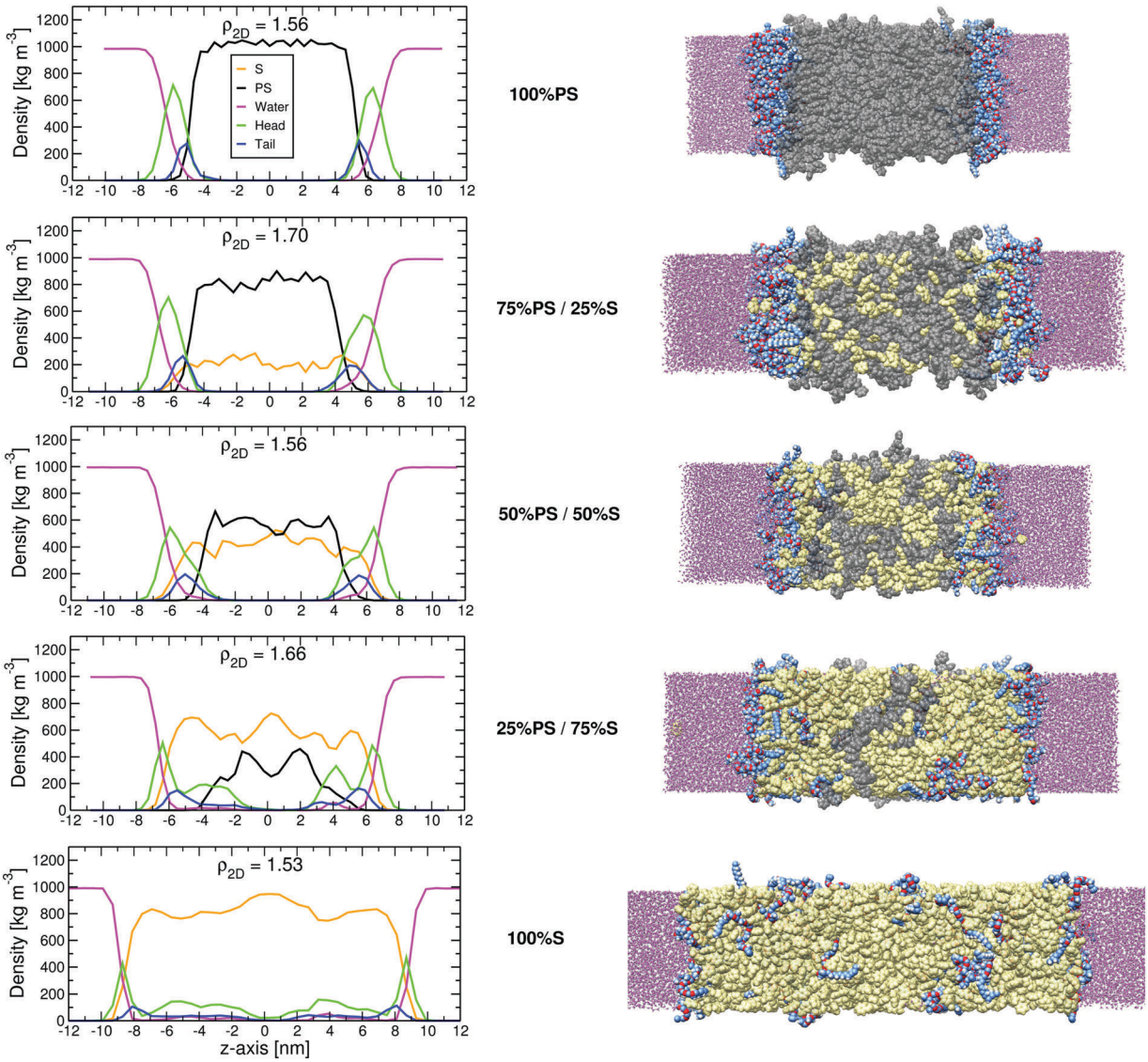

Fig. 11 Left panel: Density profiles along the z-axis for the five systems with different PS/S binary compositions of the organic phase with the nonionic surfactant 10PEO6PE. The surfactants were placed initially at the two interfaces at 2D-density of 1.61 ± 0.09 mg m^{-2} and their profiles are decomposed into heads and tails. Right panel: A snapshot of the last configuration of the corresponding simulations. Color code is the same as in Fig. 10.

and 100% S, respectively. Above these points, we observe a direct correlation between the surfactant concentration in the organic phase with that at the interface. The curve for 100% S seems to be linear (with a correlation coefficient of 0.983) as dictated by the equality of the chemical potentials (see eqn (S3), ESI†). Furthermore, the slopes of the lines in Fig. 12a reflect the propensities of the different organic phases to absorb the surfactants. In Fig. S8 and eqn (S7) (ESI†) we show that the system with 75% S absorbs more, and the system with 50% S absorbs less, surfactants than the amount predicted based on a linear interpolation of the composition of styrene and PS in the organic phase.

Note that our system contains three media in which the surfactant can accumulate, and therefore, there is another equilibrium between the surfactants at the interface and those in the aqueous phase. In fact experimentally, this equilibrium is more relevant to the changes observed during emulsion polymerization (*e.g.* Fig. 2). In previous work[13] we found that only at high densities of the surfactant at the interface does the difference in free energies between adsorption at the interface and dissolution in the aqueous phase is small enough to support significant partitioning into water. Thus, these two equilibria set in successively and not in parallel. In other words, the accumulation of surfactant in the water phase will start only after the adsorption (at the interface) and absorption (inside the organic phase) reached their maximum capacities. This maximum amount of surfactant, $\Gamma_{\max}$, is estimated by,

$$\Gamma_{\max} = \rho_{2D,\max}A + \rho_{3D,\max}V, \quad (3)$$

where A is the total interfacial area and V is the total volume of the organic phase. By extrapolating the data shown in Fig. 12a to the point which corresponds approximately to the maximum

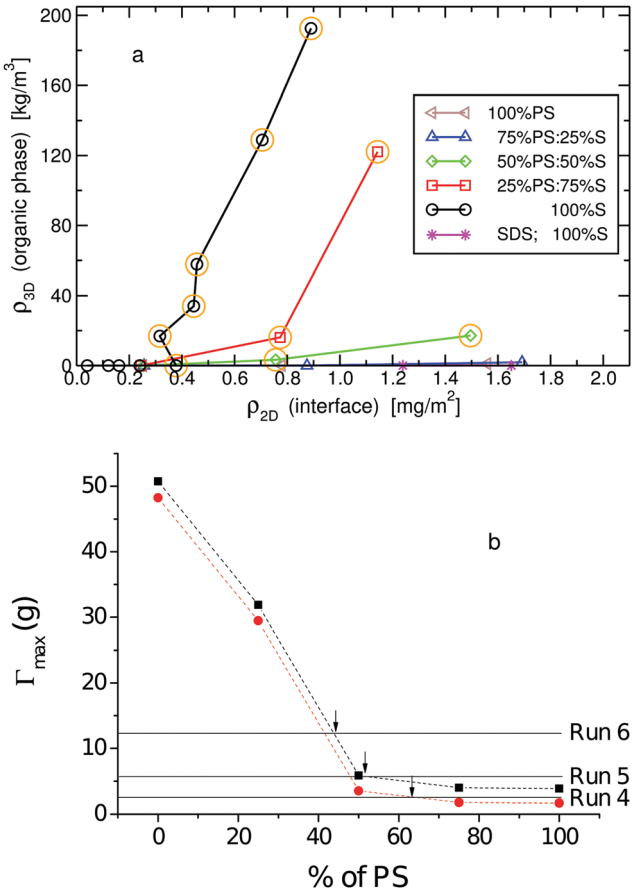

Fig. 12 (a) The density of the 10PEO6PE nonionic surfactant absorbed inside the organic phase as a function of its density adsorbed at the interface in equilibrium. Note that whereas the former is calculated using the three-dimensional volume of the organic phase the latter uses the two-dimensional area of the interface. The different curves corresponds to different chemical compositions of the organic phase. Data points surrounded by orange circles were considered for subsequent analysis in Fig. S8 (ESI†). Results from simulations of SDS ionic surfactant with 100% styrene as the organic phase are also shown. (b) Correlation of the maximum amount of 10PEO6PE surfactant that can be both adsorbed at the interface and absorbed into the organic phase, Γ_{max}, with varying PS content. In these calculations we considered the mass of the organic phase the same as in the experiment (100 g) and the diameter of the particles to be 250 nm (black squares) and 600 nm (red circles). The amounts of surfactant used in emulsion polymerizations using Disponil AFX 1080 corresponding to the Runs 4, 5 and 6 from Table 1 are denoted by horizontal lines.

packing density of the surfactant ($\rho_{2D,max}$ = 1.6 mg m^{-2}), the value of (organic phase) can be obtained. Fig. 12b shows the variation of for varying PS fraction. The different curves correspond to particles with different diameters, yet under the constraint that the total mass of the organic phase is constant and equals 100 g (see experimental conditions in Table 1). At low PS content large amounts of surfactant can be absorbed into the organic phase and hence the value of Γ_{max} is large. As the PS content increases, Γ_{max} decreases substantially and above 75% PS its value remains practically constant with all surfactant being adsorbed at the interface and no absorption occurring. The value of Γ_{max} is also affected by the particle size, with smaller particle sizes having higher surface area for adsorption, but as the total organic phase volume is constant, the extent of absorption into the organic phase is not affected.

We now relate the value of Γ_{max} obtained from the simulation to the observation of a conversion dependent secondary nucleation step in the emulsion polymerization of styrene. When the amount of surfactant in the system is less than Γ_{max}, all surfactant molecules are removed from the aqueous phase and occupy the particles' interface and potentially also their interior. However, when the amount of surfactant in the system is greater than Γ_{max}, excess surfactant will reside in the aqueous phase. Secondary nucleation occurs as a result of an increase in concentration of surfactant in the aqueous phase, thus, the point at which Γ_{max} becomes smaller than the total amount of surfactant introduced to the system should signifies the onset of secondary nucleation. In Fig. 12b the amounts of surfactant used in Runs 4, 5 and 6 (see Table 1) are shown as horizontal lines and the intersection points with the curves of Γ_{max}, accounted by the particle size, are marked by arrows. It can be seen that these points are at PS content of approximately 63%, 50% and 45% for Run 4, 5 and 6, respectively, which corresponds well with the observation of the occurrence of secondary nucleation in the emulsion polymerization at conversions of approximately 65%, 55% and 40% as shown in Fig. 2.

The penalty for the surfactant to enter the organic phase is the loss of hydrogen bonds between the head groups and the aqueous solution. To partially render the surfactant intrusion easier, water molecules accompanied this absorption process as evidenced in the density profiles in Fig. 11. In Fig. 13 we calculated the number of water molecules absorbed inside the organic phase (applying the same criteria described above for the surfactant) and plotted it against the number of absorbed surfactants. A strong correlation is evidenced for the three systems exhibiting surfactant absorption. If we approximate the curves as straight lines we find from the slopes that the number of accompanying water molecules per surfactant is 1.3, 2.8, and 5.0 for the systems with 50% S, 75% S, and 100% S, respectively.

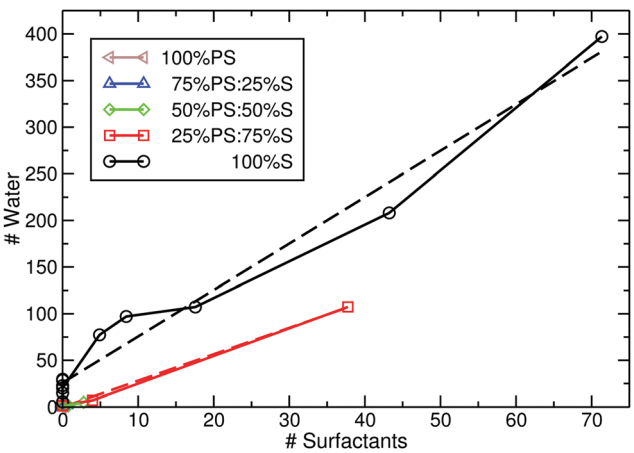

Fig. 13 The number of water molecules as a function of the number of surfactants, both of which are absorbed inside the organic phase. The corresponding dashed lines are linear regression fits.

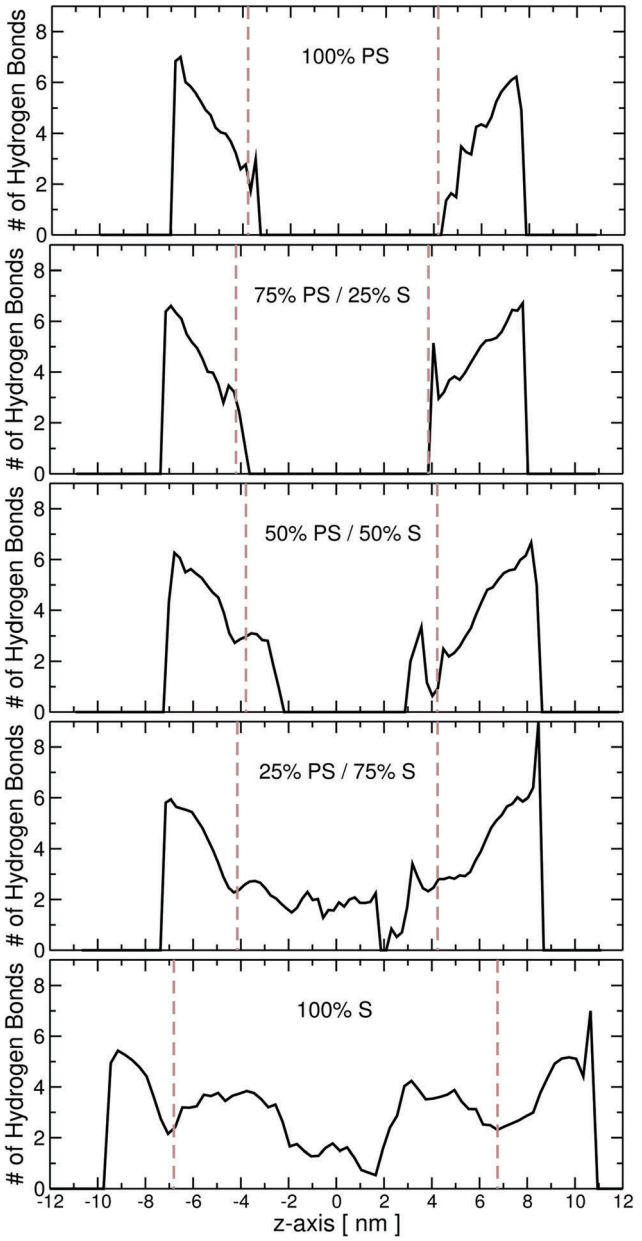

Fig. 14 The average number of hydrogen bonds (per surfactant) the nonionic surfactant forms with its surrounding water molecules as a function of its z-axis (as determined by z-coordinate of its first tail carbon atom covalently bonded to the oxygen atom of the head) for the five different organic phases for the systems shown in Fig. 11. The region between the dashed brown vertical lines denotes the location we considered to be the interior of the organic phase.

In Fig. 14 we plot the number of hydrogen bonds the head group of the surfactant forms with the surrounding water molecules as a function of the surfactant position along the z-axis. Although there is a reduction in the number of hydrogen bonds compared with the values observed at the interface, the interaction between the absorbed surfactant and the intruding water molecules is still substantial ranging from four to two hydrogen bonds per surfactant. Note that even when no surfactant is absorbed inside the organic phase or adsorbed at the interface, the number of water

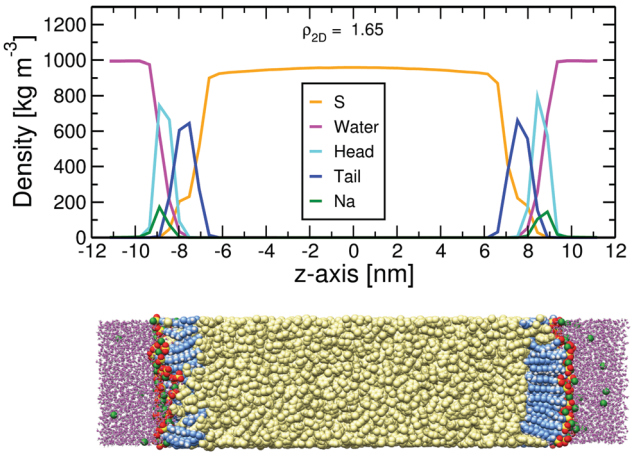

Fig. 15 The density profile along the z-axis (upper panel) and a snapshot of the last configuration (lower panel) for the simulations with SDS surfactants at 2D-density of 1.65 mg m^{-2}. The color code is the same as in Fig. 10, sulfur atoms of SDS and the sodium counterions are shown as yellow and green spheres, respectively. Similar results, of no absorption of SDS into the styrene phase, were also obtained with a lower 2D-density of 1.24 mg m^{-2}.

molecules inside the organic phase, albeit at low concentrations, is not zero. This is shown in Fig. S9 (ESI†) which reveals a sharp increase in the water density inside the organic phase of 100% S reaching a value of 1.5–3.0 kg m^{-3} which is larger by a factor of 2.5–5.0 than that found experimentally.[37]

We also performed similar simulations with 100% S for the organic phase but instead of 10PEO6PE we used SDS as the surfactant. Here, in contrast to the results for the nonionic surfactant, no absorption (zero density) into styrene was observed and the density distributions of the head and tail of SDS are clearly confined only to the interface region (Fig. 15). Given that 100% S is the organic phase with the highest propensity to absorb the nonionic surfactant, we anticipate to observe zero densities also for systems containing any mixture of styrene and PS. As we found in our previous study,[13] the self-assembly of SDS at the interface is very ordered (compared with that of the PEO–PE block copolymer surfactants), and similarly, we attribute its exclusion from a styrene-rich organic phase to its small and strongly hydrophilic head group. Such a physico-chemical character of the head group would impose a large energetic barrier upon intrusion into a medium with a low dielectric constant. Why then, the nonionic surfactant is able to absorb into styrene and not into PS. We speculate it is because at room temperature styrene is liquid whereas PS is solid. This relationship of states between monomers and their corresponding polymers is likely to be the same for other materials, and therefore, the effect induced by ionic and nonionic surfactants during the course of the polymerization reaction is anticipated to be similar to that described in this work.

Conclusions

In conclusion, we have demonstrated that nonionic surfactants, such as poly(ethylene glycol)–poly(ethylene) block copolymers,

exhibit substantially different behavior in emulsion polymerization as compared to the widely employed ionic surfactant SDS. The emulsion polymerization with nonionic surfactants is characterized by an increase in the rate of polymerization and a second nucleation period, which can be related to an unexpected increase in the surfactant concentration at advanced stages of the reaction. This can be explained by the partitioning of the surfactant into the styrene-rich phase followed by its release as the reaction progresses and the organic phase becomes rich in poly(styrene). Using atomistic molecular dynamics simulations, it was shown that when adsorbed above a critical concentration at the interface nonionic surfactants can absorb into the hydrophobic medium. For hydrophobic phases with mixed compositions of styrene and poly(styrene), we found the onset of surfactant partitioning at a content around (or just above) 50% styrene. Alongside the dissolution of the surfactant, water molecules penetrate the hydrophobic phase as well. The number of accompanying water molecules per surfactant depends on the composition of the hydrophobic medium. For ionic surfactants, such as SDS, no absorbance of surfactant has been observed under any conditions (*e.g.* neat styrene at high surfactant concentrations). It is likely that nonionic surfactants are able to absorb into these styrene-rich organic phases because their head groups are not strongly hydrophilic rendering the energetic penalty, relatively, small.

Conflicts of interest

There are no conflicts to declare.

Acknowledgements

This work has been funded with support from the Diputación Foral de Gipuzkoa, University of the Basque Country UPV/EHU (UFI 11/56), Basque Government (GVIT373-10), and the Spanish Ministry of Economy and Competitiveness (grant number CTQ2016-80886-R). We would like to also thank the technical and human support of the computer cluster provided by IZO-SGI SGIker of UPV/EHU and European funding (ERDF and ESF).

References

1 R. G. Gilbert, *Emulsion Polymerization: A Mechanistic Approach, Colloid Science*, Academic Press, London, 1995.
2 C. Chern, Emulsion polymerization mechanisms and kinetics, *Prog. Polym. Sci.*, 2006, **31**, 443–486.
3 J. M. Asua, *Polymer Reaction Engineering*, Blackwell Publishing Ltd, 2007.
4 J. L. Keddie, Film formation of latex, *Mater. Sci. Eng., R*, 1997, **21**, 101–170.
5 W. V. Smith and R. H. Ewart, Kinetics of Emulsion Polymerization, *J. Chem. Phys.*, 1948, **16**, 592–599.
6 I. Piirma and M. Chang, Emulsion polymerization of styrene: Nucleation studies with nonionic emulsifier, *J. Polym. Sci., Polym. Chem. Ed.*, 1982, **20**, 489–498.
7 I. Piirma and T. S. Maw, Emulsion polymerization: some nonionic emulsifier effects, *Polym. Bull.*, 1984, **11**, 497–504.
8 E. Özdeğer, E. D. Sudol, M. S. El-Aasser and A. Klein, Role of the nonionic surfactant Triton X-405 in emulsion polymerization. I. Homopolymerization of styrene, *J. Polym. Sci., Part A: Polym. Chem.*, 1997, **35**, 3813–3825.
9 M. Okubo, H. Kobayashi, T. Matoba and Y. Oshima, Incorporation of Nonionic Emulsifiers Inside Particles in Emulsion Polymerization: Mechanism and Methods of Suppression, *Langmuir*, 2006, **22**, 8727–8731.
10 H. Kobayashi, E. Miyanaga and M. Okubo, Preparation of Multihollow Polymer Particles by Seeded Emulsion Polymerization Using Seed Particles with Incorporated Nonionic Emulsifier, *Langmuir*, 2007, **23**, 8703–8708.
11 M. Okubo, H. Kobayashi, C. Huang, E. Miyanaga and T. Suzuki, Water Absorption Behavior of Polystyrene Particles Prepared by Emulsion Polymerization with Nonionic Emulsifiers and Innovative Easy Synthesis of Hollow Particles, *Langmuir*, 2017, **33**, 3468–3475.
12 N. Ballard, J. Urrutia, S. Eizagirre, T. Schäfer, G. Diaconu, J. C. de la Cal and J. M. Asua, Surfactant Kinetics and Their Importance in Nucleation Events in (Mini)emulsion Polymerization Revealed by Quartz Crystal Microbalance with Dissipation Monitoring, *Langmuir*, 2014, **30**, 9053–9062.
13 G. M. Meconi, N. Ballard, J. M. Asua and R. Zangi, Adsorption and Desorption Behavior of Ionic and Nonionic Surfactants on Polymer Surfaces, *Soft Matter*, 2016, **12**, 9692–9704.
14 J. Chanda and S. Bandyopadhyay, Molecular Dynamics Study of a Surfactant Monolayer Adsorbed at the Air/Water Interface, *J. Chem. Theory Comput.*, 2005, **1**, 963–971.
15 N. R. Tummala, L. Shi and A. Striolo, Molecular dynamics simulations of surfactants at the silica-water interface: Anionic vs nonionic headgroups, *J. Colloid Interface Sci.*, 2011, **362**, 135–143.
16 Z. Li, A. K. V. Dyk, S. J. Fitzwater, K. A. Fichthorn and S. T. Milner, Atomistic Molecular Dynamics Simulations of Charged Latex Particle Surfaces in Aqueous Solution, *Langmuir*, 2016, **32**, 428–441.
17 R. Wu, X. Qiu, Y. Shi and M. Deng, Molecular dynamics simulation of the atomistic monolayer structures of *N*-acyl amino acid-based surfactants, *Mol. Simul.*, 2017, **43**, 491–501.
18 K. Esselink, P. Hilbers, N. van Os, B. Smit and S. Karaborni, Molecular dynamics simulations of model oil/water/surfactant systems, *Colloids Surf., A*, 1994, **91**, 155–167.
19 J. Chen and J. Hao, Molecular dynamics simulation of cetyltrimethylammonium bromide and sodium octyl sulfate mixtures: aggregate shape and local surfactant distribution, *Phys. Chem. Chem. Phys.*, 2013, **15**, 5563–5571.
20 X. Tang, P. H. Koenig and R. G. Larson, Molecular Dynamics Simulations of Sodium Dodecyl Sulfate Micelles in Water – The Effect of the Force Field, *J. Phys. Chem. B*, 2014, **118**, 3864–3880.

21 C. Yang and H. Sun, Surface-Bulk Partition of Surfactants Predicted by Molecular Dynamics Simulations, *J. Phys. Chem. B*, 2014, **118**, 10695–10703.
22 H. W. Horn, W. C. Swope, J. W. Pitera, J. D. Madura, T. J. Dick, G. L. Hura and T. Head-Gordon, Development of an improved four-site water model for biomolecular simulations: TIP4P-Ew, *J. Chem. Phys.*, 2004, **120**, 9665–9678.
23 Z. Li, K. A. Fichthorn and S. T. Milner, Surfactant binding to polymer–water interfaces in atomistic simulations, *Langmuir*, 2016, **32**, 7519–7529.
24 B. Hess, C. Kutzner, D. van der Spoel and E. Lindahl, GROMACS 4: Algorithms for Highly Efficient, Load-Balanced, and Scalable Molecular Simulation, *J. Chem. Theory Comput.*, 2008, **4**, 435–447.
25 G. Bussi, D. Donadio and M. Parrinello, Canonical Sampling through Velocity Rescaling, *J. Chem. Phys.*, 2007, **126**, 014101.
26 H. J. C. Berendsen, J. P. M. Postma, W. F. van Gunsteren, A. DiNola and J. R. Haak, Molecular Dynamics with Coupling to An External Bath, *J. Chem. Phys.*, 1984, **81**, 3684–3690.
27 T. Darden, D. York and L. Pedersen, Particle Mesh Ewald: An N-log(N) Method for Ewald Sums in Large Systems, *J. Chem. Phys.*, 1993, **98**, 10089–10092.
28 U. Essmann, L. Perera, M. L. Berkowitz, T. Darden, H. Lee and L. G. Pedersen, A Smooth Particle Mesh Ewald Method, *J. Chem. Phys.*, 1995, **103**, 8577–8593.
29 S. Miyamoto and P. A. Kollman, SETTLE: An Analytical Version of the SHAKE and RATTLE Algorithms for Rigid Water Models, *J. Comput. Chem.*, 1992, **13**, 952–962.
30 B. Hess, H. Bekker, H. J. C. Berendsen and J. G. E. M. Fraaije, LINCS: A Linear Constraint Solver for Molecular Simulations, *J. Comput. Chem.*, 1997, **18**, 1463–1472.
31 A. Luzar and D. Chandler, Structure and hydrogen bond dynamics of water-dimethyl sulfoxide mixtures by computer simulations, *J. Chem. Phys.*, 1993, **98**, 8160–8173.
32 P. Mukerjee and K. J. Mysels, *Critical Micelle Concentrations of Aqueous Surfactant Systems*, U.S. National Bureau of Standards, Washington, DC, 1971.
33 D. C. Sundberg, J. Y. Hsieh, S. K. Soh and R. F. Baldus, *Diffusion-Controlled Kinetics in the Emulsion Polymerization of Styrene and Methyl Methacrylate*, American Chemical Society, Washington, D.C., 1981, ch. 20, pp. 327–343.
34 A. M. Fernandez, U. Held, A. Willing and W. H. Breuer, New green surfactants for emulsion polymerization, *Prog. Org. Coat.*, 2005, **53**, 246–255.
35 J. d. S. Nunes and J. M. Asua, Theory-Guided Strategy for Nanolatex Synthesis, *Langmuir*, 2012, **28**, 7333–7342.
36 S. Sajjadi, Nanoparticle Formation by Monomer-Starved Semi-batch Emulsion Polymerization, *Langmuir*, 2007, **23**, 1018–1024.
37 W. Lane, Determination of Solubility of Styrene in Water and of Water in Styrene, *Ind. Eng. Chem., Anal. Ed.*, 1946, **18**, 295–296.

Electronic Supplementary Material (ESI) for Physical Chemistry Chemical Physics.

Supplementary Information: Shedding Light on the Different Behavior of Ionic and Nonionic Surfactants in Emulsion Polymerization: From Atomistic Simulations to Experimental Observations

Giulia Magi Meconi[1], Nicholas Ballard[1], José M. Asua[1], and Ronen Zangi*[2,3]

[1]POLYMAT & Departamento de Química Aplicada, Facultad de Ciencias Químicas, University of the Basque Country UPV/EHU, Avenida de Tolosa 72, 20018, Donostia–San Sebastián, Spain

[2]POLYMAT & Departamento de Química Orgánica I, University of the Basque Country UPV/EHU, Avenida de Tolosa 72, 20018, Donostia–San Sebastián, Spain

[3]IKERBASQUE, Basque Foundation for Science, María Díaz de Haro 3, 48013 Bilbao, Spain

October 31, 2017

*Email: r.zangi@ikerbasque.org

Table S1: Details of the simulations for the five organic phases (different composition of PS and styrene) studied. For each organic phase, we considered four concentrations (eleven for 100% S) of 10PEO6PE surfactants. The average lengths of the simulation box along each axis are indicated (the interfaces between water and the organic phase are normal to the z-axis). The values of the 2D-densities, ρ_{2D}, are initial values which do not take into consideration absorption into the organic phase at equilibrium. For the system with 100% S the box lengths in the x- and y-axes are the same.

	# 16-mer PS	# S	# 10PEO6PE	ρ_{2D} [mg/m^2]	# Waters	$\langle X \rangle$ [nm]	$\langle Y \rangle$	$\langle Z \rangle$ [nm]
100% S	0	2304	0	0	8170	5.17	5.17	25.00
	0	2304	2	0.0405	8170	5.18	5.18	25.00
	0	2304	6	0.121	8170	5.20	5.20	25.00
	0	2304	8	0.161	8170	5.20	5.20	25.00
	0	2304	12	0.240	8170	5.22	5.22	25.00
	0	2304	18	0.378	8604	5.09	5.09	27.00
	0	2304	20	0.419	8604	5.10	5.10	27.00
	0	2304	30	0.619	8604	5.13	5.13	27.00
	0	2304	40	0.814	8604	5.17	5.17	27.00
	0	2304	80	1.53	11630	5.33	5.33	30.00
	0	2304	120	2.20	11630	5.45	5.45	30.00
25% PS / 75% S	36	1728	0	0	14208	5.64	6.74	22.00
	36	1728	18	0.244	15130	5.79	6.92	22.00
	36	1728	62	0.826	14208	5.84	6.99	22.00
	36	1728	122	1.66	11628	5.79	6.92	22.00
50% PS / 50% S	72	1152	0	0	13036	6.66	5.65	21.00
	72	1152	18	0.255	13036	6.73	5.71	21.00
	72	1152	56	0.767	12678	6.84	5.81	21.00
	72	1152	114	1.56	13308	6.83	5.80	23.00

Continued on next page

Table S1 – continued from previous page

	# 16-mer PS	# S	# 10PEO6PE	ρ_{2D} [mg/m^2]	# Waters	$\langle X \rangle$ [nm]	$\langle Y \rangle$	$\langle Z \rangle$ [nm]
75% PS / 25% S	108	576	0	0	14392	6.79	5.50	22.00
	108	576	18	0.256	14392	6.87	5.56	22.00
	108	576	62	0.875	13138	6.90	5.59	22.00
	108	576	124	1.70	11892	7.00	5.67	22.00
100% PS	144	0	0	0	13238	6.35	5.94	21.00
	144	0	18	0.252	13238	6.45	6.03	20.84
	144	0	56	0.779	12148	6.47	6.04	20.86
	144	0	112	1.56	10404	6.45	6.03	21.00

Table S2: Details of the simulation setups for the SDS surfactants studied at two different 2D-densities with 100% S as the organic phase. The data collection time was 20 ns, and the equilibration time was 80 and 100 ns for the systems with 146 and 200 SDSs, respectively. The box lengths in the x- and y-axes are the same.

# SDS	ρ_{2D} [mg/m^2]	# S	# Waters	$\langle X \rangle / \langle Y \rangle$ [nm]	$\langle Z \rangle$ [nm]
146	1.24	2304	5286	5.31	22.80
200	1.65	2304	5203	5.39	22.80

Table S3: Details of the simulation setups for the calculations of the potential of mean force of pulling one 10PEO6PE surfactant adsorbed at the interface to the water phase. The different densities, reported as ρ_{2D}, correspond to different numbers of surfactants initially placed at the interface.

# 10PEO6PE	ρ_{2D} [mg/m^2]	# S	# Waters	$\langle X \rangle / \langle Y \rangle$ [nm]	$\langle Z \rangle$ [nm]
1	0.0538	384	4113	4.50	9.70
8	0.453	384	11452	4.38	22.04
12	0.686	384	8006	4.36	17.05

Models for Styrene and Poly(styrene)

The bonded and non-bonded parameters for styrene and PS were taken from the OPLS-AA force-field of ethylbenzene and ethylene molecules.[1–3] However for PS, in order to allow the connectivity between the subunits and simultaneously maintain zero charge for each of these subunits, we made the following changes. The partial charge of C_β of the first residue was changed from -0.180 to -0.120, that of C_γ of the last residue was changed from -0.115 to -0.055, and both changes were applied to the repeating residues. The chain of PS is modeled as a 16-mer unit. Because the stereochemistry of each unit is randomly generated during polymerization, we chose to model each chain with alternating C_α chiral centers (R followed by S). The resulting model is shown in Fig. S1 and the non-bonded interactions are specified in Table S4. Using this model, we obtained a value of 1.02 kg/m^3 for the density of amorphous PS which is close to its experimental value[4] of 1.04–1.06 kg/m^3. Furthermore, the calculated values of the radius of gyration, 9.8 Å, and the weight-normalized end-to-end distance squared, 0.42 Å$^2\cdot$ mol/g, are also in a very good agreement with their experimentally determined values of 10.0 Å and 0.43 Å$^2\cdot$ mol/g, respectively.

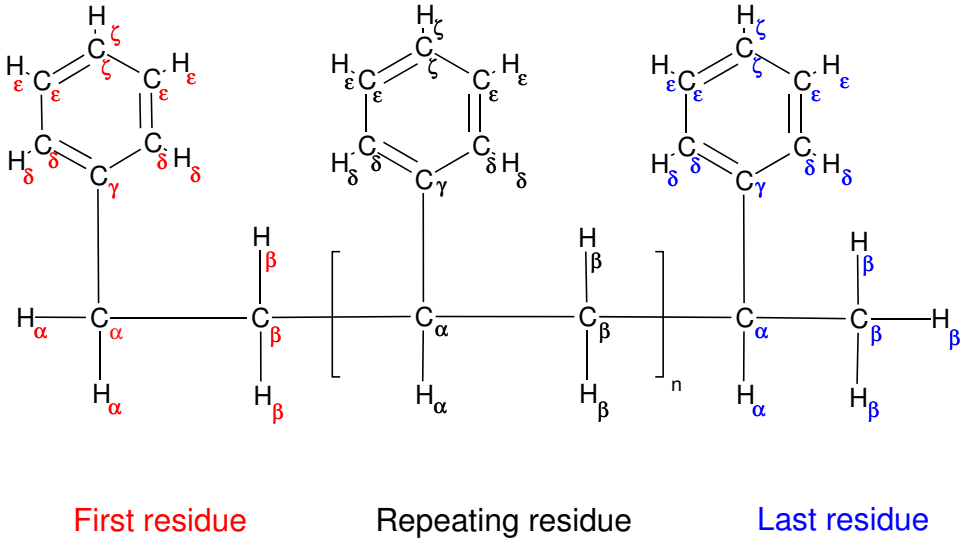

Figure S1: The model for PS based on the OPLS-AA force-field. The partial charge and LJ parameters describing each atom are detailed in Table S4. Note that the C_α of the repeating and last residues are chirals, nevertheless, the parameters for the R and S configurations are the same.

Table S4: Partial charges and LJ parameters for the PS model. The values refer to all residue types (first, repeating, and last) unless otherwise indicated.

	q [e]	σ [nm]	ϵ [kJ/mol]
C_α	-0.005	0.350	0.276
C_β	-0.120	0.350	0.276
$C_{\beta,\text{last}}$	-0.180	0.350	0.276
C_γ	-0.055	0.355	0.293
$C_{\gamma,\text{first}}$	-0.115	0.355	0.293
H_α, H_β	+0.060	0.250	0.126
C_δ, C_ϵ, C_ζ	-0.115	0.355	0.293
H_δ, H_ϵ, H_ζ	+0.115	0.242	0.126

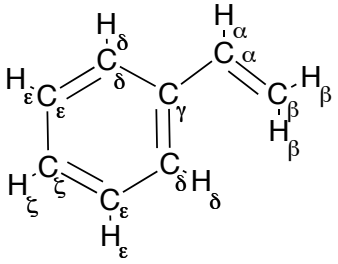

Figure S2: The model for a styrene molecule. The OPLS-AA partial charges and LJ parameters are detailed in Table S5.

Table S5: Partial charges and LJ parameters for styrene.

	q [e]	σ [nm]	ϵ [kJ/mol]
C_α	-0.115	0.355	0.318
C_β	-0.230	0.355	0.318
C_γ	-0.115	0.355	0.293
H_α	+0.23	0.242	0.126
H_β	+0.115	0.242	0.126
C_δ, C_ϵ, C_ζ	-0.115	0.355	0.293
H_δ, H_ϵ, H_ζ	+0.115	0.242	0.126

A Model for poly(ethylene oxide)-poly(ethylene)

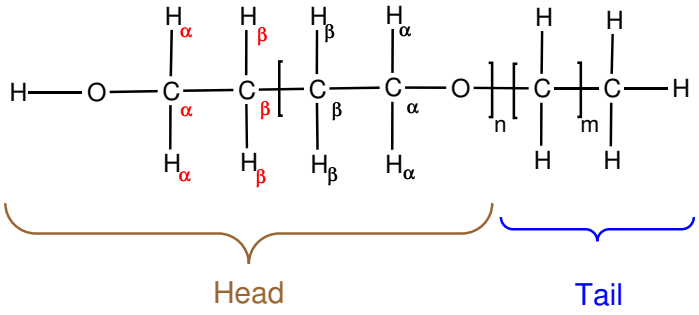

Figure S3: The model for 10PEO6PE surfactant (n=10 and m=11). The partial charges and LJ parameters, taken from the OPLS-AA force-field, are detailed in Table S6. For PEO, the values were based on a dimethyl ether.

Table S6: Partial charges and LJ parameters for the PEO-PE surfactant model. The atoms are divided according to their association to the head or tail groups.

	q [e]	σ [nm]	ϵ [kJ/mol]
Head			
$C_{\alpha,\beta}$	+0.140	0.350	0.276
$C_{\alpha,first}$	-0.015	0.350	0.276
$H_{\alpha,\beta}$	+0.030	0.250	0.126
$H_{\alpha,first}$	+0.040	0.250	0.126
O	-0.400	0.290	0.586
O_{first}	-0.683	0.312	0.711
H_{first}	+0.418	0.000	0.000
Tail			
C	-0.120	0.350	0.276
C_{last}	-0.180	0.350	0.276
H	+0.060	0.250	0.126

A Model for Sodium Dodecyl Sulfate

Partial charges, bonded and nonbonded parameters for SDS were adopted from the model of Shelley et al.[5,6]. Note that this model integrates the hydrogens of the methyl and methylene groups into the carbons to which they are connected. To obtain an all-atom representation, we represented the atom-types and partial charges of methyl and methylene groups by the OPLS-AA force-field for hydrocarbons. The sum of the charges for each of these groups is zero, therefore, in order to determine the partial charges of the first methylene group (which has a total charge of $+0.137$ e), we performed quantum calculations (using the Gaussian09 software[7] at the MP2/6-31++G**) and followed the RESP (Restrained Electrostatic Potential) charge fitting procedure[8]. Bonded interactions that were missing for the all-atom description were taken from the corresponding interactions of the OPLS-AA force-field. The resulting model is displayed in Fig. S4 and the non-bonded parameters in Table S7 The LJ parameters of the sodium counterion, σ=0.333 nm and ϵ=0.0116 kJ/mol, were taken from the OPLS-AA force-field. Note that the charges obtained by RESP reproduce the, quantum mechanically determined, electrostatic potential at large number of grid points around the optimized geometry of the molecule. Thus, their values can differ substantially from the atomic charges determined quantum mechanically (e.g, as defined by Mulliken) for the same optimized molecular structrure (see Fig. S5).

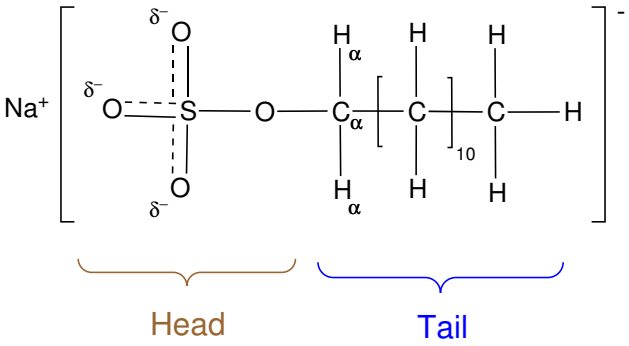

Figure S4: The model for SDS surfactant. The partial charge and LJ parameters describing each atom are detailed in Table S7.

Table S7: Partial charges and LJ parameters for the SDS model. The atoms are divided according to their association to the head or tail groups.

	q [e]	σ [nm]	ϵ [kJ/mol]
Head			
S	+1.284	0.355	1.046
O	-0.654	0.315	0.837
O_{ester}	-0.459	0.300	0.711
Tail			
C_α	+0.077	0.350	0.276
H_α	+0.030	0.242	0.063
C	-0.120	0.350	0.276
C_{last}	-0.180	0.350	0.276
H	+0.060	0.250	0.126

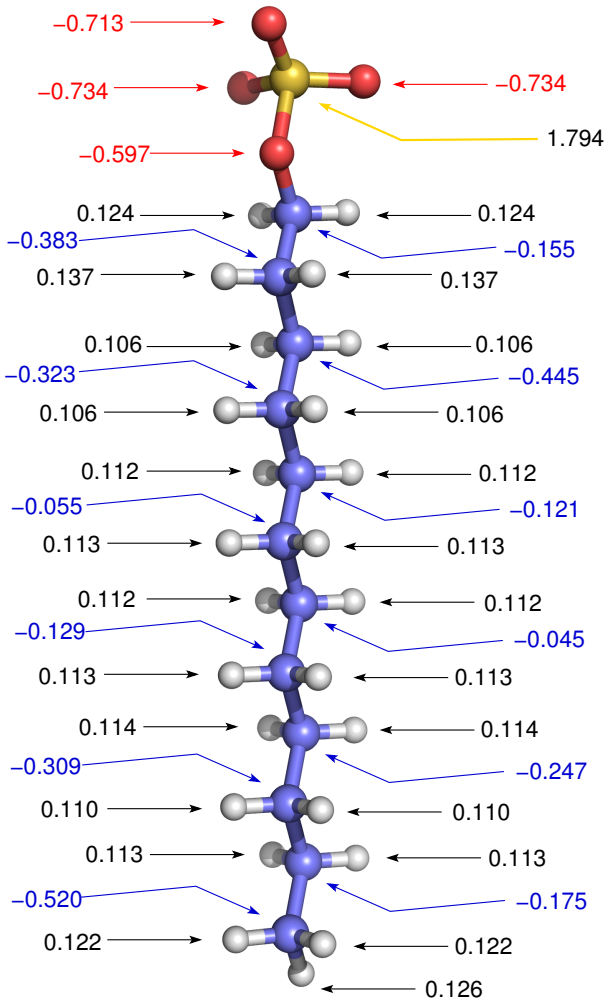

Figure S5: Atomic (Mulliken) charges (in elementary charge units, *e*) for the dodecyl sulfate anion optimized quantum mechanically at the MP2/6-31++G** level. These charges were *not* used in the classical simulations.

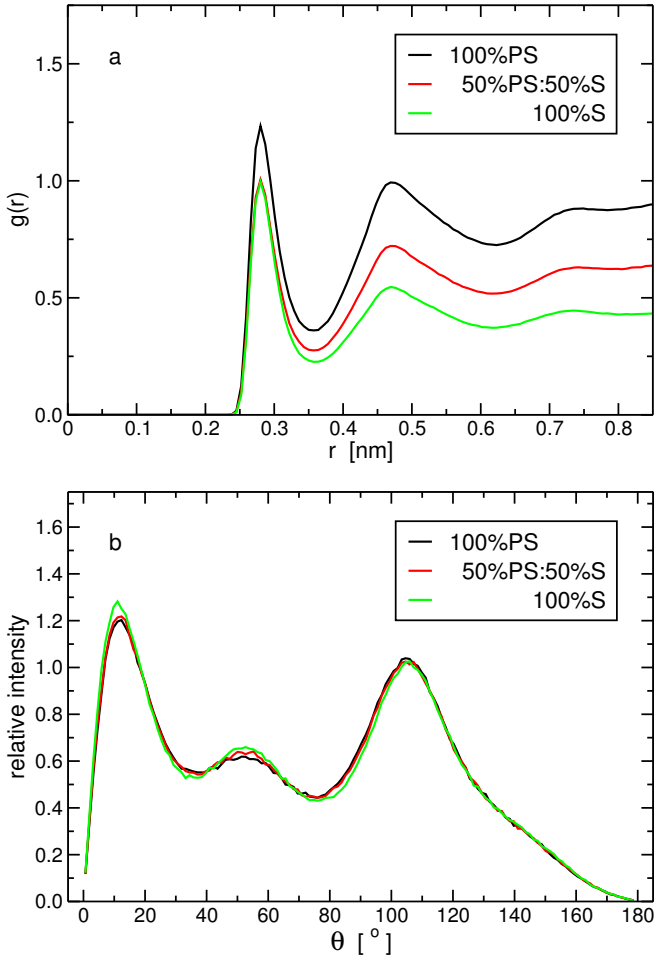

Figure S6: (a) The radial distribution function between the oxygen atoms of the nonionic surfactant and the oxygen atoms of the water molecules. (b) The distribution of the angle formed by the hydrogen–oxygen(water)–oxygen(surfactant) atomic sites for donor–acceptor distances smaller than 0.35 nm. For both plots, the corresponding distributions were calculated for three different chemical compositions of the organic phase.

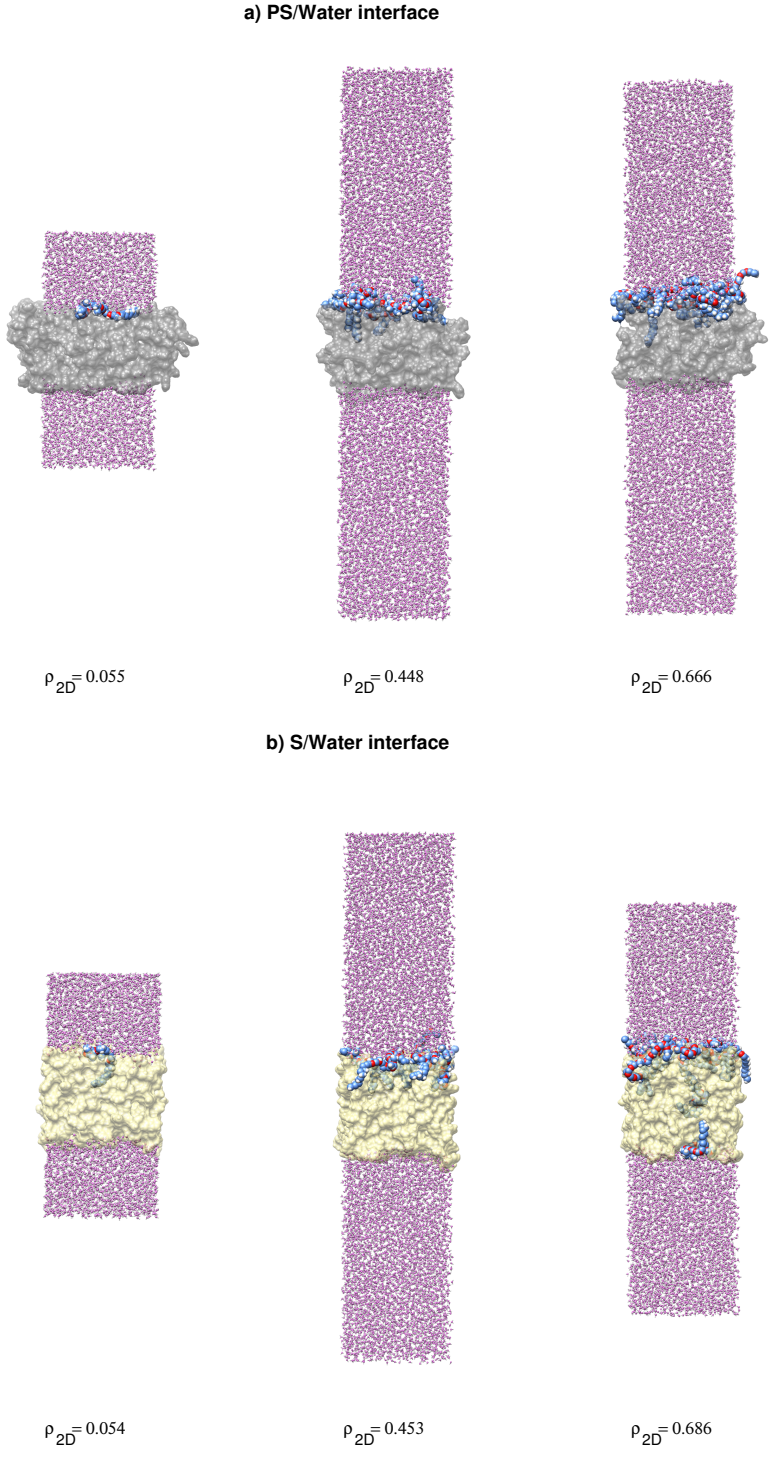

Figure S7: Same as Fig. 10, however here, the entire length of the simulation box along the z-axis (normal to the interface) is shown for all snapshots.

Relation between the Surfactant Densities at the Interface and inside the Organic Phase

The chemical potential of the surfactant in the organic phase is given by,

$$\mu_{\mathsf{op}} = \mu_{\mathsf{op}}^{\ominus} + \mathsf{RT} \ln \mathsf{a}_{\mathsf{op}} = \mu_{\mathsf{op}}^{\ominus} + \mathsf{RT} \ln \left[\gamma_{\mathsf{op}} \frac{\rho_{\mathsf{op}}}{\rho_{\mathsf{op}}^{\ominus}} \right] \quad , \tag{S1}$$

where $\mu_{\mathsf{op}}^{\ominus}$ is the chemical potential in the organic phase under standard conditions of temperature, pressure, and density. The term a_{op} is the activity of the surfactants relative to the standard state, which can be written in terms of the activity coefficient, γ_{op}, and the surfactant density relative to that chosen for the standard state. A corresponding term holds at the interface,

$$\mu_{\mathsf{int}} = \mu_{\mathsf{int}}^{\ominus} + \mathsf{RT} \ln \left[\gamma_{\mathsf{int}} \frac{\rho_{\mathsf{int}}}{\rho_{\mathsf{int}}^{\ominus}} \right] \quad . \tag{S2}$$

At equilibrium, $\mu_{\mathsf{op}} = \mu_{\mathsf{int}}$, from which we get,

$$\rho_{\mathsf{op}} = \frac{\gamma_{\mathsf{int}}}{\gamma_{\mathsf{op}}} \cdot \frac{\rho_{\mathsf{op}}^{\ominus}}{\rho_{\mathsf{int}}^{\ominus}} \exp \left[- \left(\mu_{\mathsf{op}}^{\ominus} - \mu_{\mathsf{int}}^{\ominus} \right) / \mathsf{RT} \right] \rho_{\mathsf{int}} \quad . \tag{S3}$$

The terms associated with the standard states and the activity coefficients are constants with respect to the concentration of the surfactant, and therefore, a plot of ρ_{op} as a function of ρ_{int} should yield a straight line as obtained in Fig. 12a. Note that the lines do not pass through the origin, because below the critical density the surfactant does not absorb into the organic phase and the there is no equality between the chemical potentials (i.e., Eq. S3 does not hold). In fact in this case, the chemical potential of the surfactant in the organic phase is larger than that in that at the interface.

Taking the derivative of Eq. S3 with respect to ρ_{int} on both sides of Eq. S3 yields,

$$\frac{\mathsf{d}\rho_{\mathsf{op}}}{\mathsf{d}\rho_{\mathsf{int}}} = \frac{\gamma_{\mathsf{int}}}{\gamma_{\mathsf{op}}} \cdot \frac{\rho_{\mathsf{op}}^{\ominus}}{\rho_{\mathsf{int}}^{\ominus}} \exp \left[- \left(\mu_{\mathsf{op}}^{\ominus} - \mu_{\mathsf{int}}^{\ominus} \right) / \mathsf{RT} \right] \quad , \tag{S4}$$

which can also be written as,

$$\ln \left[\frac{\mathsf{d}\rho_{\mathsf{op}}}{\mathsf{d}\rho_{\mathsf{int}}} \right] = \mu_{\mathsf{int}}^{\ominus} / \mathsf{RT} + \ln \left[\frac{\gamma_{\mathsf{int}}}{\gamma_{\mathsf{op}}} \cdot \frac{\rho_{\mathsf{op}}^{\ominus}}{\rho_{\mathsf{int}}^{\ominus}} \right] - \mu_{\mathsf{op}}^{\ominus} / \mathsf{RT} \quad . \tag{S5}$$

Note that, in principle, for different organic phases $\mu_{\mathsf{int}}^{\ominus}$ is different. Nevertheless in our systems for which the surfactant exhibits non-zero density inside the organic phase, it is almost exclusively styrene that is found at the interface with water (see Fig. 11 for 100% S, 75% S, and 50% S). Because of this observation we consider that $\mu_{\mathsf{int}}^{\ominus}$ and γ_{int} are independent of these three organic phases. In addition, we also make

the assumption that the value of γ_{op}, which represents the degree of deviation from an ideal behavior, is the same for these systems.

Under these two assumptions, Eq. S5 indicates that the natural logarithm of the slopes of the lines in Fig. 12a, for different chemical compositions of the organic phase, are only a function of $\mu^{\ominus}_{op}$ where all other terms enter as constant parameters. For an organic phase composed of styrene and PS, one may naively try to relate $\mu^{\ominus}_{op}$ to the chemical potential of styrene in the standard state, $\mu^{\ominus}_{str}$, and that of PS, $\mu^{\ominus}_{ps}$, weighted linearly by the corresponding fractions in the organic phase, χ_{str} and 1 - χ_{str}, respectively.

$$\mu^{\ominus}_{op} \simeq \chi_{str}\mu^{\ominus}_{str} + (1-\chi_{str})\mu^{\ominus}_{ps} \tag{S6}$$

In such a case, Eq. S5 becomes,

$$\ln\left[\frac{d\rho_{op}}{d\rho_{int}}\right] = \left(\mu^{\ominus}_{int} - \mu^{\ominus}_{ps}\right)/RT + \ln\left[\frac{\gamma_{int}}{\gamma_{op}}\cdot\frac{\rho^{\ominus}_{op}}{\rho^{\ominus}_{int}}\right] - \left(\mu^{\ominus}_{str} - \mu^{\ominus}_{ps}\right)/RT\cdot\chi_{str} \quad . \tag{S7}$$

Thus, plotting $\ln\left[\frac{d\rho_{op}}{d\rho_{int}}\right]$ as a function of χ_{str} should yield a straight line with a slope equals -$\left(\mu^{\ominus}_{str} - \mu^{\ominus}_{ps}\right)/RT$. This is plotted in Fig. S8 for the three organic phases containing non-zero surfactant density.

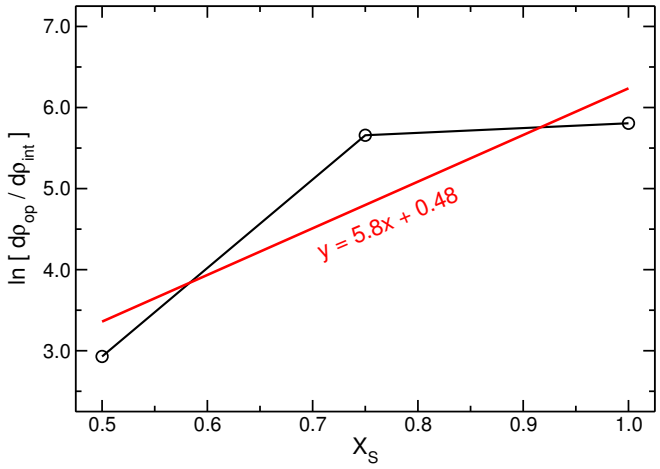

Figure S8: The natural logarithm of the slopes of the lines shown in Fig. 12a (for 100% S, 75% S, and 50% S) as a function of the mass fraction of styrene in the organic phase (see Eq. S7). Only points surrounded by orange circles in Fig. 12a are used for the calculations of the slopes. The red line is a linear regression obtained with a correlation coefficient of 0.888.

The slope of 5.8 of the linear regression means that $\mu^{\ominus}_{\mathsf{str}}$ is smaller by 5.8 RT than $\mu^{\ominus}_{\mathsf{ps}}$, which is in agreement with the observation that the surfactant absorbs significantly more in the styrene phase relative to the PS phase. Nevertheless, the relatively small correlation coefficient for the linear fitting suggests that $\mu^{\ominus}_{\mathsf{op}}$ deviates from the simplistic expression we assumed, and/or the value of γ_{op} varies for the three organic phases. In particular, for 75% S the organic phase resembles 100% S more than expected based on linear interpolation of the mass fractions of the two components, whereas for 50% S, it resembles less.

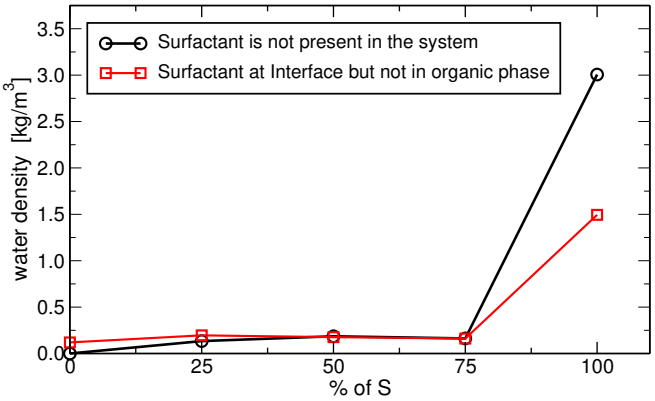

Figure S9: The density of the water molecules inside the organic phase as a function of the percentage of styrene composing the organic phase. The data are plotted for cases in which no surfactant (10PEO6PE) is either present at all in the system or absorbed inside the organic phase (but adsorb at the interface). For the latter, we chose the system with the highest density of surfactant at the interface that does not support absorbance into the organic phase.

References

[1] Jorgensen, W. L.; Severance, D. L. Aromatic-Aromatic Interactions: Free Energy Profiles for the Benzene Dimer in Water, Chloroform and Liquid Benzene, *J. Am. Chem. Soc.* **1990**, *112*, 4768–4774.

[2] Jorgensen, W. L.; Maxwell, D. S.; .; Tirado-Rives, J. Development and Testing of the OPLS All-Atom Force Field on Conformational Energetics and Properties of Organic Liquids, *J. Am. Chem. Soc.* **1996**, *118*, 11225–11236.

[3] Price, M. L. P.; Ostrovsky, D.; Jorgensen, W. L. Gas-Phase and Liquid-State Properties of Esters, Nitriles, and Nitro Compounds with the OPLS-AA Force Field, *J. Comp. Chem.* **2001**, *22*, 1340–1352.

[4] Brandrup, J.; Immergut, E. H.; Grulke, E. A. *Polymer Handbook;* Wiley: New York, fourth ed., 2003.

[5] Shelley, J.; Watanabe, K.; Klein, M. L. Simulation of a sodium dodecylsulfate micelle in aqueous solution, *Int. J. Quant. Chem.* **1990**, *38*, 103–117.

[6] Schweighofer, K. J.; Essmann, U.; Berkowitz, M. Simulation of Sodium Dodecyl Sulfate at the Water-Vapor and Water-Carbon Tetrachloride Interfaces at Low Surface Coverage, *J. Phys. Chem. B* **1997**, *101*, 3793–3799.

[7] Gaussian 09 Revision A.02. Frisch, M. J.; Trucks, G. W.; Schlegel, H. B.; Scuseria, G. E.; Robb, M. A.; Cheeseman, J. R.; Scalmani, G.; Barone, V.; Mennucci, B.; Petersson, G. A.; Nakatsuji, H.; Caricato, M.; Li, X.; Hratchian, H. P.; Izmaylov, A. F.; Bloino, J.; Zheng, G.; Sonnenberg, J. L.; Hada, M.; Ehara, M.; Toyota, K.; Fukuda, R.; Hasegawa, J.; Ishida, M.; Nakajima, T.; Honda, Y.; Kitao, O.; Nakai, H.; Vreven, T.; Montgomery, Jr., J. A.; Peralta, J. E.; Ogliaro, F.; Bearpark, M.; Heyd, J. J.; Brothers, E.; Kudin, K. N.; Staroverov, V. N.; Kobayashi, R.; Normand, J.; Raghavachari, K.; Rendell, A.; Burant, J. C.; Iyengar, S. S.; Tomasi, J.; Cossi, M.; Rega, N.; Millam, J. M.; Klene, M.; Knox, J. E.; Cross, J. B.; Bakken, V.; Adamo, C.; Jaramillo, J.; Gomperts, R.; Stratmann, R. E.; Yazyev, O.; Austin, A. J.; Cammi, R.; Pomelli, C.; Ochterski, J. W.; Martin, R. L.; Morokuma, K.; Zakrzewski, V. G.; Voth, G. A.; Salvador, P.; Dannenberg, J. J.; Dapprich, S.; Daniels, A. D.; Farkas, Ö.; Foresman, J. B.; Ortiz, J. V.; Cioslowski, J.; Fox, D. J.; Gaussian, Inc., Wallingford, CT, **2009**.

[8] Bayly, C. I.; Cieplak, P.; Cornell, W.; Kollman, P. A. A well-behaved electrostatic potential based method using charge restraints for deriving atomic charges: the RESP model, *J. Phys. Chem.* **1993**, *97*, 10269–10280.